Neuroradiology (2010) 52:785–807
DOI 10.1007/s00234-010-0742-1

TOPIC ARTICLE

Diffusion-weighted magnetic resonance imaging of the temporal bone

B. De Foer · J-P. Vercruysse · M. Spaepen · T. Somers · M. Pouillon · E. Offeciers · J. W. Casselman

Received: 23 June 2010 / Accepted: 25 June 2010 / Published online: 15 July 2010

Abstract This paper summarizes the value of diffusion-weighted magnetic resonance imaging in the evaluation of temporal bone pathology. It highlights the use of different types of diffusion-weighted magnetic resonance imaging in the different types of cholesteatoma, prior to first stage surgery and prior to second look surgery. The value of diffusion-weighted magnetic resonance imaging in the evaluation of pathology of the apex of the petrous bone and the cerebellopontine angle is also discussed.

Keywords Temporal bone · Magnetic resonance imaging · CT · Diffusion-weighted MRI · Cholesteatoma · Petrous apex · Cholesterol granuloma · Pneumatization of petrous apex · Cerebellopontine angle · Epidermoid

Introduction

Image evaluation of diseases of the temporal bone has till now mainly been guided by clinical and audiological findings. One can state that conductive hearing loss is mainly evaluated using computed tomography (CT) and that sensorineural hearing loss is mainly examined using magnetic resonance imaging (MRI).

Most pathologies causing conductive hearing loss are situated in the middle ear whereas most causes of sensorineural hearing loss are found in the inner ear or in the central auditory pathways.

However, this somewhat artificial subdivision in image evaluation of pathology of the temporal bone has become more vague for the past few years due to newer technical developments in MRI, such as diffusion-weighted (DW) MRI.

MRI and more specifically DW MRI have gained increasing importance in the evaluation of pathology of the entire temporal bone region.

This review aims to provide an overview of the current status of the published data on DW MRI in the temporal bone region.

A short introduction of this technique is provided followed by the current status in the evaluation of middle ear lesions and cholesteatoma more specifically. The appearance of the most frequent lesions of the petrous bone apex and cerebellopontine angle (CPA) on DW MRI will also be discussed.

B. De Foer (✉) · M. Spaepen · M. Pouillon · J. W. Casselman
Department of Radiology, GZA Hospitals Sint-Augustinus,
Oosterveldlaan 24,
2610 Wilrijk (Antwerp), Belgium
e-mail: bert.defoer@GZA.be

J.-P. Vercruysse · T. Somers · E. Offeciers
University Department of ENT, GZA Hospitals Sint-Augustinus,
Oosterveldlaan 24,
2610 Wilrijk (Antwerp), Belgium

J. W. Casselman
Department of Radiology, AZ Sint-Jan AV,
Ruddershove 10,
8000 Bruges, Belgium

Diffusion-weighted magnetic resonance imaging

The mechanism of DW MRI is based on the Brownian motion of water molecules in tissue and, more importantly, on the hindrances/facilitations of water molecule movements in various types of tissue. In order to make an MRI sequence sensitive to the diffusion of water molecules, the sequence is expanded with a diffusion-sensitizing gradient scheme, usually a very fast, single-shot gradient-echo data collecting sequence (echoplanar—EP). The amount of diffusion sensitizing applied is usually indicated by the *b*-

value. In clinical practice, images are generally acquired with a *b*-value of 0 and 1,000 s/mm^2 [1, 2].

However, numerous artefacts can be generated during acquisition of DW MRI, such as eddy current artefacts, susceptibility artefacts, ghosting artefacts, chemical shift, and motion artefacts [3]. With the use of higher magnetic fields, these artefacts and image distortions on EP DW imaging are even more pronounced.

Due to the low incidence of movement artefact, the high brain homogeneity and high signal-to-noise ratio research at the onset was mainly focused on the brain.

This resulted in the fact that clinically, DW MR imaging is an established method used routinely for the diagnosis of acute stroke [1, 2].

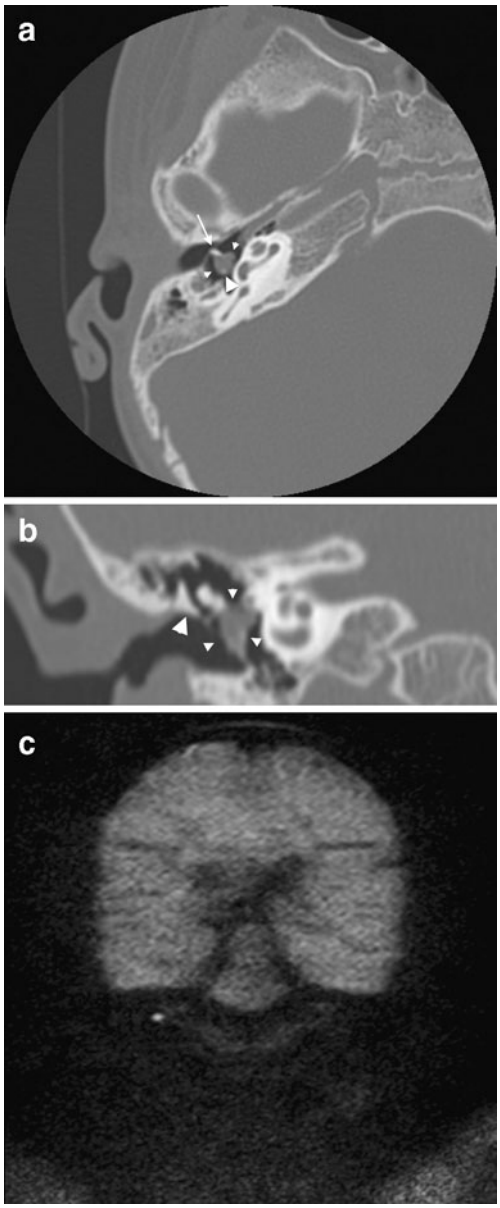

Fig. 1 A 12-year-old boy presenting with conductive hearing loss and a suspicion of a congenital cholesteatoma at otoscopy. **a** Axial CT image at the level of the basal turn of the cochlea. Small nodular soft tissue (*small arrowheads*) between the handle of the malleus (*arrow*) and the long process of the incus (*large arrowhead*). **b** Coronal reformatted CT image at the level of the cochlea. Small nodular soft tissue (*small arrowheads*) in the mesotympanum. Note that Prussak's space is free and well aerated and that the scutum is sharp (*large arrowhead*). **c** Coronal non-EP DW b1000 image (SS TSE DW sequence or HASTE DW sequence). Small nodular hyperintensity compatible with a small congenital cholesteatoma. Conclusion: Small congenital cholesteatoma

Fig. 2 A 47-year-old male presenting with a long-standing deafness on the left side and a sudden onset of facial nerve palsy. **a** Axial CT scan at the level of the geniculate ganglion, vestibule, and lateral semicircular canal. There is a large lytic lesion centered on the geniculate ganglion (*large arrows*). The lesion has a component protruding in the anterior epitympanic space with erosion of the malleus head (*small arrow*). The labyrinthine segment of the facial nerve canal can no longer be delineated suggestive of extension and/or invasion along this segment of the facial nerve. **b** Axial CT scan at the level of the superior semicircular canal. The lesion is situated anterior and lateral in the temporal bone pyramid (*arrows*). There is a "C-shaped" extension medially and posteriorly (*small arrowheads*), crossing the roof of the fundus of the internal auditory canal (*large arrowhead*). **c** Coronal reformatted CT image at the level of the cochlea. Large lytic lesion centered on the region of the geniculate ganglion (*small arrowheads*) with a large component extending in the middle ear epitympanic space (*large arrowheads*) with erosion of the malleus head (*arrow*). **d** Axial 0.4-mm-thick 3D TSE T2-weighted image at the level of the internal auditory canal. The most striking feature is the asymmetrical signal intensity in the internal auditory canal. The signal intensity is much lower in the left internal auditory canal (*small arrowheads*). Moreover, the vestibulo-cochlear nerve branches and facial nerve can no longer be discriminated. Compare to the normal signal intensity in the IAC and the visible superior vestibular nerve branch on the right side (*large arrowhead*). **e** Axial gadolinium-enhanced 2-mm-thick SE T1-weighted image at the level of the left internal auditory canal. The lesion displays mixed signal intensity with enhancing as well as centrally located non-enhancing parts (*small arrowheads*). There is also some peripheral enhancement in the internal auditory canal (*large arrowhead*). **f** Coronal gadolinium-enhanced 2-mm-thick SE T1-weighted image at the level of the left internal auditory canal. The lesion displays mixed signal intensities with enhancing and centrally located non-enhancing parts (*small arrowheads*). There is also some enhancement noted at the periphery of the internal auditory canal (*large arrowheads*). **g** Coronal 2-mm-thick TSE T2-weighted image at the level of the internal auditory canal (same level as **f**). The lesion demonstrates a moderate intensity with a "C-shaped" extension towards the roof of the internal auditory canal (*small arrowheads*). **h** Coronal non-EP DW b1000 image (SS TSE DW sequence or HASTE DW sequence) (same level as **f** and **g**) nicely demonstrating the lesion in the epitympanum (*large arrowhead*) underneath the temporal lobe, the "C-shaped" extension towards the internal auditory canal (*small arrowhead*) and the extension into the internal auditory canal (*arrow*). Conclusion: Congenital cholesteatoma with characteristic location centered on the geniculate ganglion. There is a component protruding into the middle ear which can also be regarded as highly typical for a congenital cholesteatoma. There is medial extension along the course of the facial nerve and probably also via the "C-shaped" extension towards the internal auditory canal. The extension in the internal auditory canal can be seen on the 3D TSE T2-weighted sequence as well as the non-EP DW sequence. The clear hyperintensity on this last sequence confirms the diagnosis of a congenital cholesteatoma

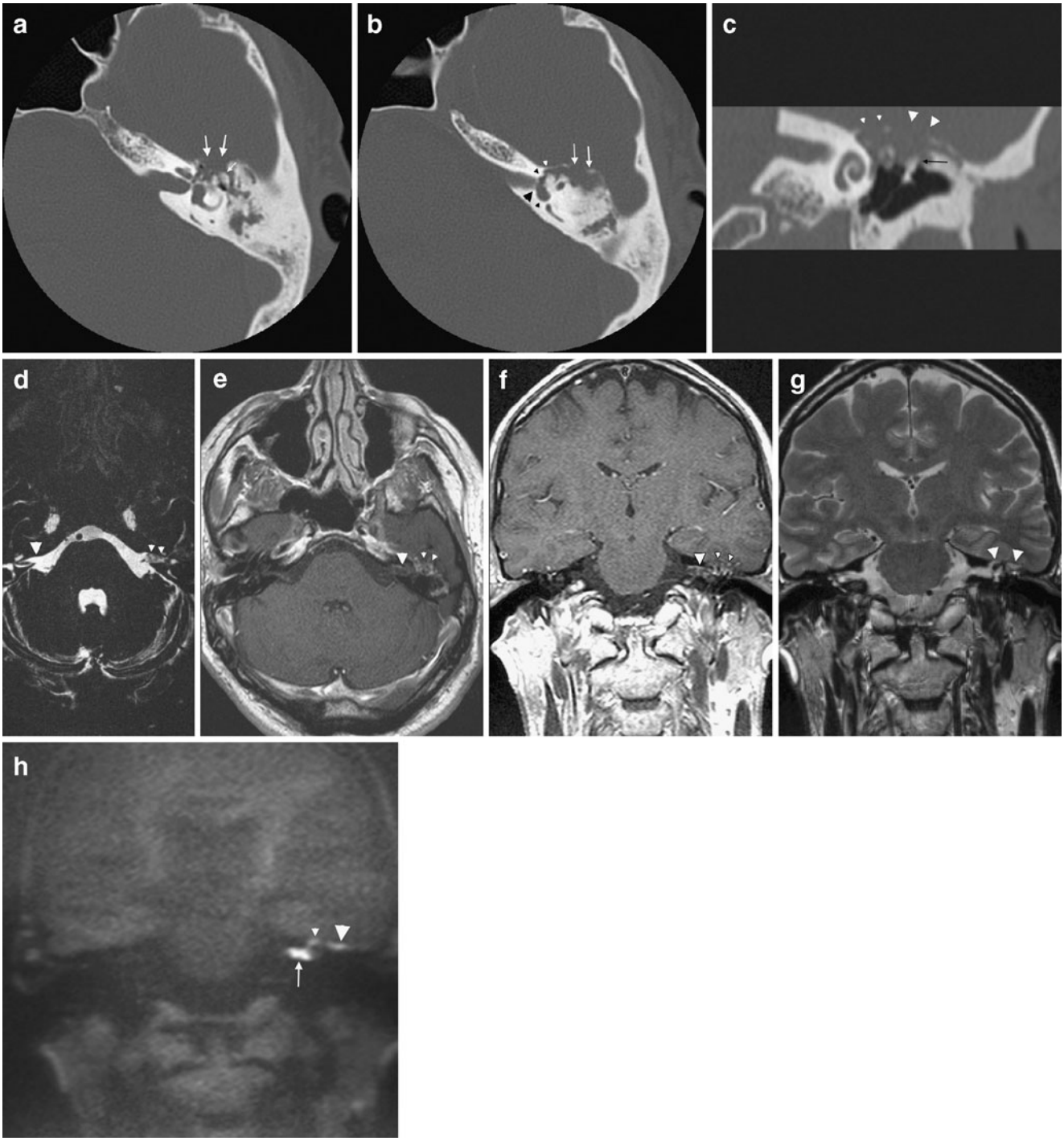

However, over the last few years, several extracranial applications of DW MRI have been developed. Major applications have been described in the diagnosis and treatment follow-up of tumoral lesions in the upper abdomen, pelvis, and head and neck region [1].

In the temporal bone region, the interface between air, bone, and the temporal lobe is particularly prone to susceptibility artefacts [3]. For the evaluation of the temporal bone region, several types of non-echoplanar-based diffusion-weighted sequences have been described [3–5]. These turbo spin echo (TSE) or fast spin echo (FSE)-based diffusion-weighted have a higher spatial resolution, generate thinner slices (down to 2 mm), and do not suffer at all from susceptibility artefacts [3]. The single-shot turbo spin echo diffusion-weighted sequence uses a 180° radio-frequency refocusing pulse for each measured echo, which

explains the reduction of the susceptibility artefact. It permits fast multiplanar imaging in artefact-prone regions, such as the posterior fossa and the inferior frontal and temporal lobes [3].

Cholesteatoma

Congenital versus acquired cholesteatoma

Congenital cholesteatoma

Congenital cholesteatoma is a rare entity originating at the time of closure of the neural tube in which the ectoderm—the later skin—gets entrapped in the skull, extradurally, in the temporal bone [6, 7].

When the ectoderm gets entrapped in the skull intradurally, the term epidermoid cyst is used. The term epidermoid tumor is considered a misnomer as this entity is regarded as a congenital anomaly rather than a tumoral entity.

Both congenital cholesteatoma and epidermoid cyst are the same histological entity, comprised of entrapped ectoderm or skin. The lesion starts to expand by the continuous exfoliation and desquamation of the epithelium, giving rise to a slowly expansile lesion with pressure changes on the surrounding tissues. Both lesions contain exfoliated skin or keratin inside.

Congenital cholesteatoma can be found anywhere in the temporal bone pyramid. In the middle ear, it is most frequently found in the anterior superior part of the middle ear. It can extend posterior towards the ossicular chain with

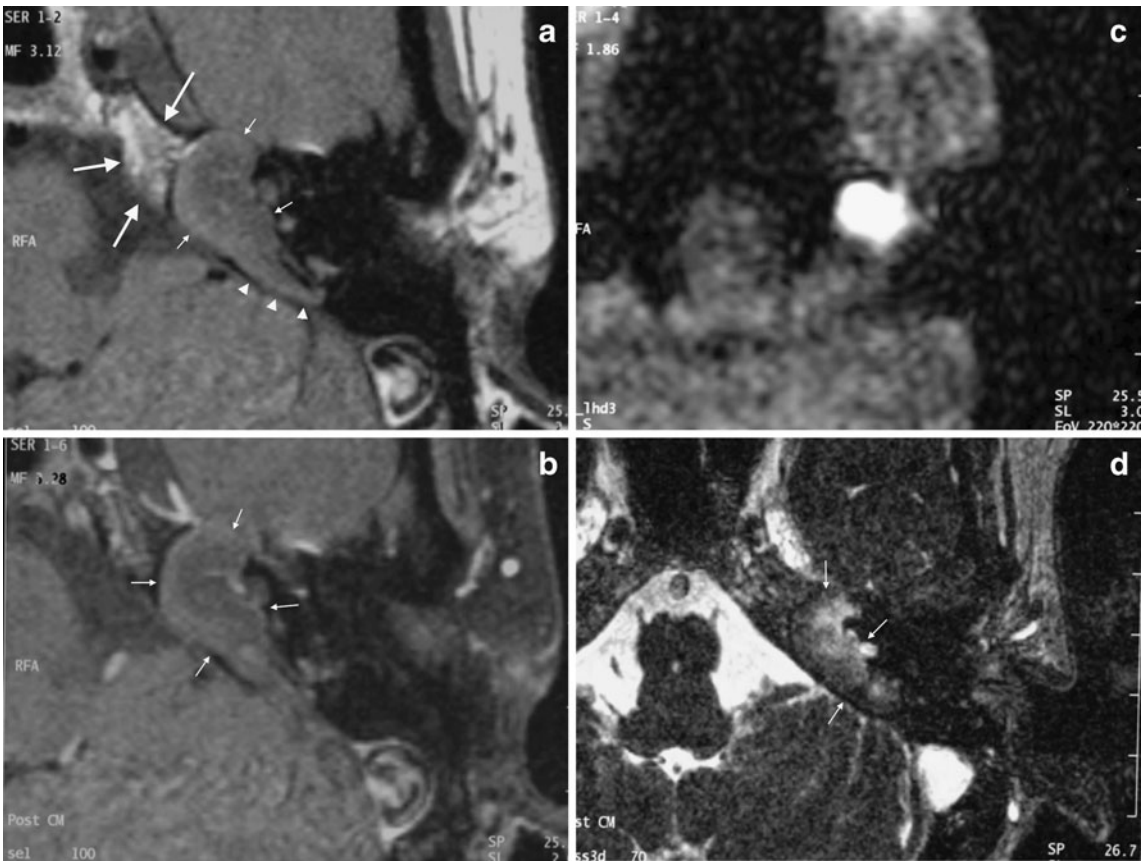

Fig. 3 A 50-year-old female investigated for headache, with a prior history of middle ear surgery on the left side for cholesteatoma. **a** Axial unenhanced T1-weighted image at the level of the apex of the left petrous bone. There is some residual fat in the apex of the left petrous bone (*large arrows*). Note the hypointense nodular lesion in the apex of the left petrous bone (*small arrows*). There is a tail-like extension of the lesion along the posteromedial border of the temporal bone (*arrowheads*). **b** Axial post-gadolinium T1-weighted image with fat suppression (same level as **a**). The lesion is not enhancing (*small arrows*). **c** Axial EP DW b1000 image. Large nodular hyperintensity in the left petrous bone apex. **d** Axial 3D CISS image at the level of the petrous bone apex. The lesion has a mixed signal intensity—hypo to moderate intense. Intensity is anyhow lower than CSF (*small arrows*). Conclusion: Signal intensity on the b1000 image is pathognomonic for a cholesteatoma in the apex of the petrous bone, as cholesteatoma is the only lesion which is displaying a clear hyperintensity on b1000 diffusion-weighted images. Signal intensities on standard sequences are also compatible with petrous bone apex cholesteatoma. Cholesteatoma of the petrous bone apex is probably a secondary cholesteatoma. Most likely, the extension is situated along the posteromedial side of the left temporal bone (Courtesy of Prof. F. Veillon, Strasbourg, France)

possible associated erosion of the ossicular chain [6, 7] (Fig. 1). By definition, a middle ear congenital cholesteatoma is found behind an intact tympanic membrane without any signs of associated infection [6, 7].

Congenital cholesteatoma can also be found in the region of the inner ear and membranous labyrinth in which it has a predilection for the region around the geniculate ganglion [6, 7] (Fig. 2). Very often, it has a component protruding in the middle ear and a component invading the membranous labyrinth. The component protruding in the middle ear is often causing a conductive hearing loss due to impingement and/or erosion of the ossicular chain. Clini-

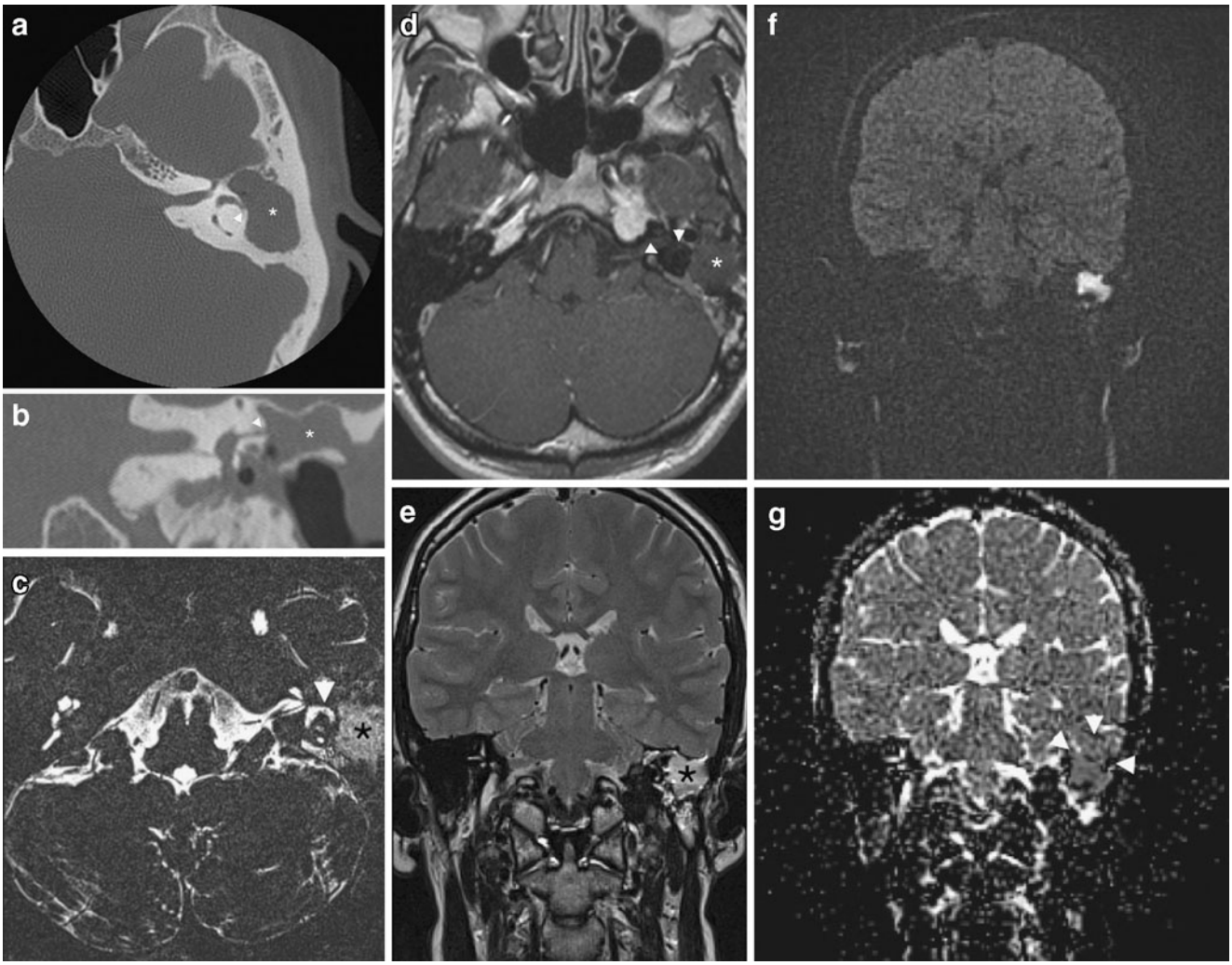

Fig. 4 A 28-year-old male presenting with acute onset of vertigo. **a** Axial CT scan at the level of the lateral semicircular canal. There is a homogeneous opacification of the left middle ear and mastoid (*asterisk*) without further discrimination of any residual ossicles or bony trabeculation. There is a possible defect in the bony wall of the lateral semicircular canal (*arrowhead*). **b** Coronal CT reformation at the level of the intersection of the superior semicircular canal, the lateral semicircular canal, and the vestibule. Soft tissues (*asterisk*) in the middle ear and mastoid with possible fistulisation towards the lateral semicircular canal (*arrowhead*). **c** Axial 0.4-mm-thick 3D TSE T2-weighted image at the level of the lateral semicircular canal. The entire middle ear is filled with a moderate intense nodular lesion (*asterisk*). Signal intensities in the membranous labyrinth and at the level of the lateral semicircular canal more specifically are normal (*arrowhead*). **d** Axial delayed post-gadolinium 2-mm-thick SE T1-weighted image at the level of the lateral semicircular canal. There is a centrally non-enhancing lesion in the middle ear and mastoid (*asterisk*) compatible with a large middle ear cholesteatoma. At present, there is no enhancement of the membranous labyrinth (*arrowheads*). **e** Coronal 2-mm-thick TSE T2-weighted image at the level of the mastoid demonstrating a large hyperintense mass lesion completely filling up the mastoid (*asterisk*). **f** Coronal 2-mm non-EP DW MR b1000 image (Multishot (MS) TSE DW sequence or BLADE DW sequence). The lesion demonstrates a clear hyperintensity. **g** Coronal ADC map (same level as **f**). The lesion has a hypointense signal on the ADC map (*arrowheads*). Conclusion: Large middle ear and mastoid cholesteatoma with typical findings on T2 and T1-weighted sequences and on non-EP diffusion-weighted imaging. There is fistulisation to the lateral semicircular canal explaining the complaints of the patient. Actually, no enhancement of the membranous labyrinth or signal loss on heavily T2-weighted sequences is seen. Note the low signal intensity on ADC maps compatible with diffusion restriction

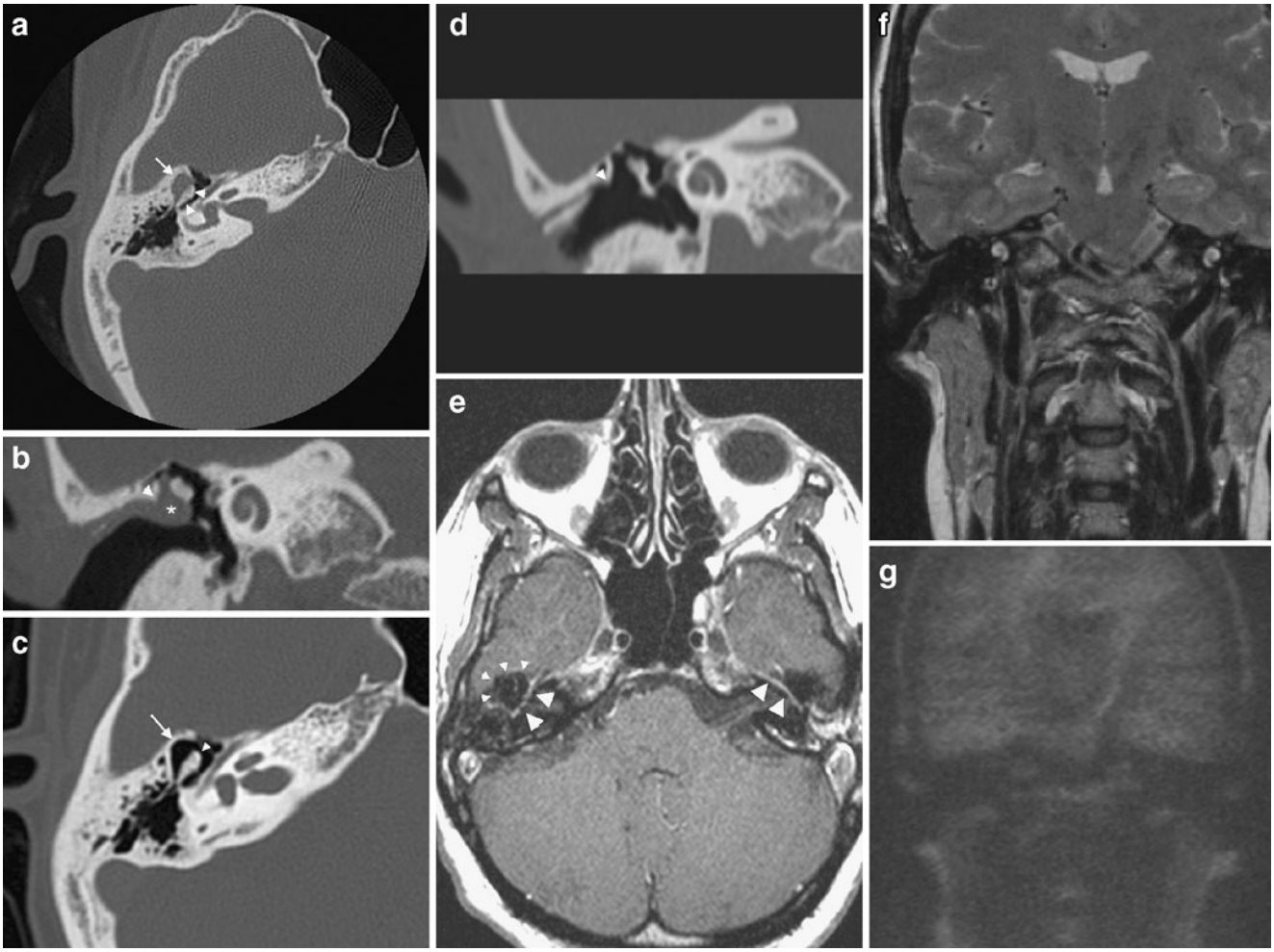

Fig. 5 A 32-year-old woman examined because of right-sided conductive hearing loss. At otoscopy, a cholesteatoma is suspected in a retraction pocket at the pars flaccida on the right side. **a** Axial CT image at the level of the malleus head, incus body, and short process. Soft tissues can be seen in Prussak's space with erosion of the lateral epitympanic wall (*arrow*), the malleus head, and incus body (*arrowheads*). **b** Coronal CT reformation at the level of the cochlea. There is a nodular soft tissue in Prussak's space (*asterisk*) with amputation of the scutum (*arrowhead*). **c** Axial CT image at the level of the malleus head, incus body, and short process (same level as **a**). CT examination performed 1 year after the CT examination in **a**. The soft tissues as seen in **a** can no longer be seen. The results of the erosion are, however, still visible: erosion of the lateral epitympanic wall (*arrow*) and the malleus head (*arrowhead*). This image is pathognomonic of an auto-evacuated cholesteatoma: the cholesteatoma sac has opened and evacuated its content through the external auditory canal. **d** Coronal reformation at the level of the cochlea (same level as **b**). CT examination performed 1 year after the CT examination in **b**. The soft tissues in Prussak's space as seen in **b** can no longer be seen. The amputation of the scutum can, however, still be seen (*arrowhead*). Again, this image is typical of an auto-evacuated cholesteatoma sac. **e** Axial delayed post-gadolinium T1-weighted image at the level of the middle ear (same level as **a** and **c**, same date of acquisition as **c**). The tympanic segment of the facial nerve can be seen on both sides (*large arrowheads*). The cholesteatoma epithelium or matrix can be suspected against the lateral epitympanic wall as a very thin enhancing line (*small arrowheads*). However, the typical central hypointensity cannot be seen due to the autoevacuation. **f** Coronal T2-weighted image at the level of the cochlea (same level as **b** and **d**, same date of acquisition as **d**). No clear hyperintensity can be seen. **g** Coronal non-EP DW (SS TSE DW sequence or HASTE DW sequence, same level as **b**, **d**, and **f**, same date of acquisition as **d** and **f**) b1000 image showing no clear hyperintensities. The lack of hyperintensity on diffusion-weighted sequences confirms the diagnosis of an auto-evacuated cholesteatoma. Conclusion: Auto-evacuated cholesteatoma confirmed by two consecutive CT scans (**a** and **b** versus **c** and **d**). In the time between both CT scans, the cholesteatoma sac has evacuated its content through the external auditory canal. The hyperintensity on DWI in case of a cholesteatoma is caused by the retained keratin in the cholesteatoma pocket. In case of auto-evacuation, the keratin gets evacuated and the hyperintensity on DWI is no longer seen. The characteristic findings on standard MRI sequences, a hyperintensity on T2-weighted images, and a hypointensity on T1-weighted images, can also not be found. The cholesteatoma epithelium or matrix is still adherent to the attic but is very difficult to visualize it, most often due to the associated infectious enhancement

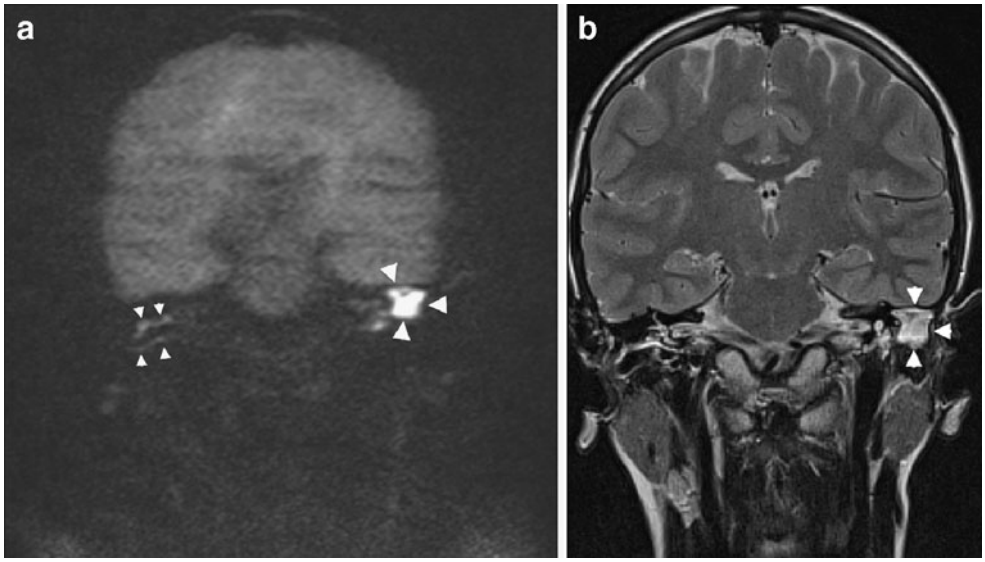

Fig. 6 A 41-year-old male with a large cholesteatoma on the left side. MR imaging performed in a preoperative setting. **a** Coronal non-EP DW b1000 image (SS TSE DW sequence or HASTE DW sequence). Large nodular hyperintensity on the left side (*large arrowheads*) compatible with a large middle ear cholesteatoma. There are two linear hyperintensities on the right side (*small arrowheads*). **b** Coronal 2-mm-thick TSE T2-weighted image at the level of the internal auditory canal demonstrating the large middle ear cholesteatoma on the left side (*large arrowheads*). Note that the linear hyperintensities as seen on the diffusion-weighted images are situated against the roof and bottom of the external auditory canal on the right side. Subsequent otoscopy revealed the presence of cerumen in the external auditory canal on the right side. Suction cleaning followed by a repeated coronal non-EP DW sequence showed disappearance of the linear hyperintensity (not shown). Conclusion: Cerumen in the external auditory canal can also present as a hyperintensity on b1000 diffusion-weighted images. The linear aspect of the hyperintensity and the location in the external auditory canal are pathognomonic for cerumen

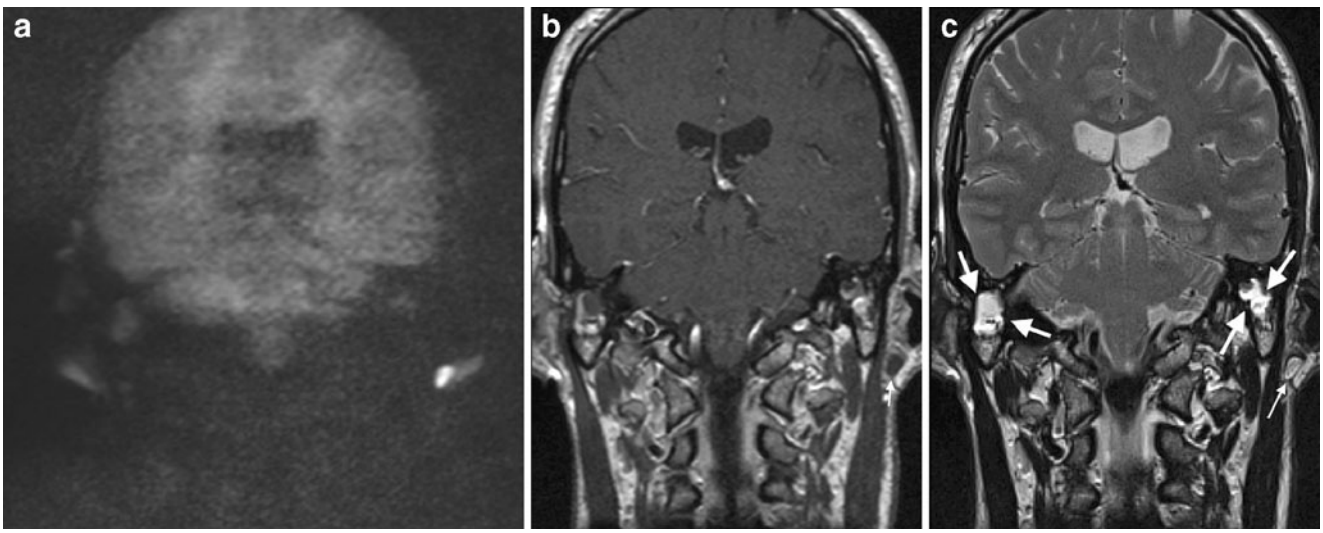

Fig. 7 Follow-up study of a 24-year-old male who previously underwent surgery for a middle ear cholesteatoma. Imaging is performed to exclude residual cholesteatoma. **a** Coronal non-EP DW b1000 image (SS TSE DW sequence or HASTE DW sequence). No clear hyperintensity can be seen on the right side. Surprisingly, a nodular hyperintensity is seen on the left side. The hyperintensity is located rather low and lateral. Correlation with ADC map (not shown) revealed a clear hypointensity of the lesion. **b** Coronal 2-mm-thick delayed post-Gd T1-weighted image (same slice position as **a**). The nodular lesion has a hypointense aspect and is situated outside the temporal bone (*small arrow*), under the earlobe of the external ear. **c** Coronal 2-mm-thick TSE T2-weighted image (same slice position as **a** and **b**). The nodular lesion can clearly be seen as a moderately intense lesion underneath the earlobe of the external ear (*small arrow*). Note the clear hyperintensity in the mastoid on both sides (*large arrows*) being far too intense to be compatible with cholesteatoma. Conclusion: Clinical examination revealed a sebum cyst behind the earlobe of the external ear. Sebum as well as cerumen (see Fig. 6) are also exfoliated skin just as cholesteatoma. Hence, they can also present with a hyperintense signal on diffusion-weighted imaging

cally, the inner ear component is very often causing signs of facial nerve palsy and/or sensorineural hearing loss. Debate still exists whether an isolated petrous bone apex congenital cholesteatoma exists, whether a petrous bone apex cholesteatoma is not always a middle ear cholesteatoma, extending into the petrous bone apex (Fig. 3).

Due to their location, surgical treatment of these congenital cholesteatoma is often very difficult. Care should be taken that in case of a component protruding in the middle ear, the inner ear component is resected in toto. Otherwise, the inner ear part of the congenital cholesteatoma will continue to grow further.

Acquired cholesteatoma

The acquired cholesteatoma is originating at a so-called retraction pocket most frequently situated at the upper and posterior part of the tympanic membrane or the pars flaccida.

This retraction pocket gradually starts to fill up Prussak's space, and when it gets sealed off, this retraction pocket is

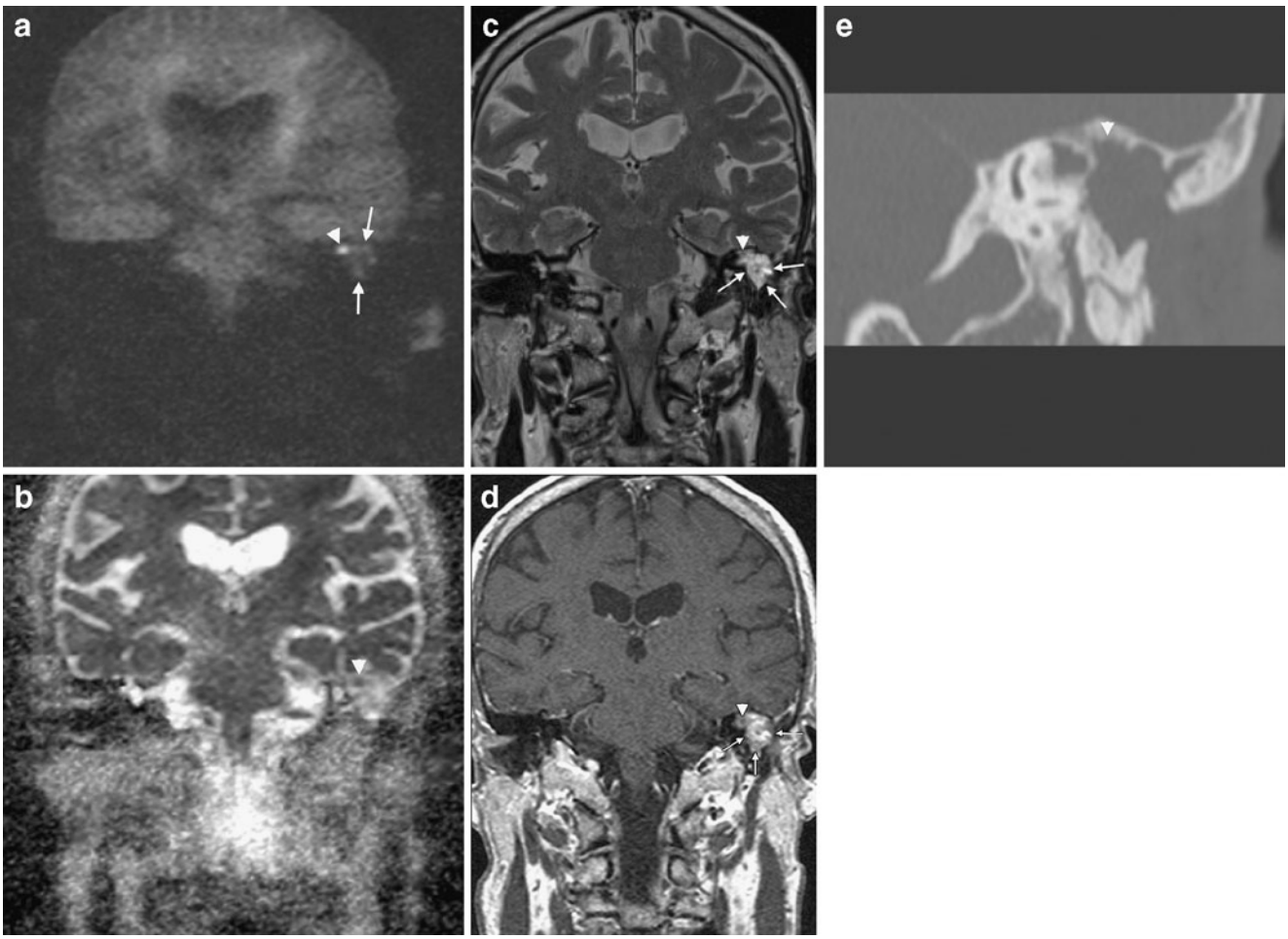

Fig. 8 A 62-year-old female treated for middle ear cholesteatoma on the left side 15 months before. **a** Coronal non-EP DW b1000 image (SS TSE DW sequence or HASTE DW sequence). A small nodular hyperintensity (*arrowhead*) is seen under the medial part of the tegmen. Note the soft tissues lateral to this nodular hyperintensity, isointense with brain tissue (*arrows*). **b** ADC map, same level as **a**. Note the small nodular hypointensity (*arrowhead*). This small nodular hypointensity corresponds to the nodular hyperintensity in **a**. **c** Coronal 2-mm-thick TSE T2-weighted image, same level as **a** and **b**. The nodular lesion can be seen as a small nodule with moderate signal intensity (*arrowhead*) delineated by clear hyperintense material on its lateral and inferior side (*arrows*). Compared to **a** and **b**. **d** Coronal 2-mm delayed post-gadolinium T1-weighted image, same level as **a**, **b**, and **c**. The lesion can be depicted as a small nodular hypointensity (*arrowhead*) under the medial part of the tegmen. It is delineated by enhancing material on its lateral and inferior side (*arrows*). Compare to **a**, **b**, and **c**. **e** Corresponding coronal CT reformation (same level as **a**–**d**). After the canal wall up tympanoplasty, the middle ear cavity is completely filled up with soft tissue. No further discrimination is possible. The lesion is probably situated medially, when correlated with MR findings(*arrowhead*). Conclusion: This case demonstrates the strength of the non-EP DW sequence in detecting very small residual cholesteatoma. On CT scan, the cholesteatoma cannot be discriminated from the surrounding postoperative soft tissues which have the same density. The lesion is—without correlation to the non-EP DW sequence—hardly discernable on standard MR sequences. Note that even on the ADC map, this very small cholesteatoma is discernable as a drop in signal intensity, making differentiation with the surrounding postoperative findings possible

gradually starting to enlarge by the continuous desquamation of the epithelium, the so-called cholesteatoma matrix [8, 9].

Growing slowly, this pars flaccida cholesteatoma will start eroding surrounding structures. It will start to erode the scutum—the bony spur of Prussak's space—and the ossicular chain at the level of the malleus head and the body and short process of the incus. The lateral epitympanic wall can also be eroded. By further expanding, the ossicular chain is displaced medially in case of a pars flaccida cholesteatoma [8, 9].

When the cholesteatoma expands further, it gradually fills up the attic towards the mastoid and it can erode several structures with possible complications. Extension towards the roof of the middle ear cavity can erode the tegmen with possible invasion into the middle cranial fossa and subsequent complications of meningitis or a temporal lobe abscess [8].

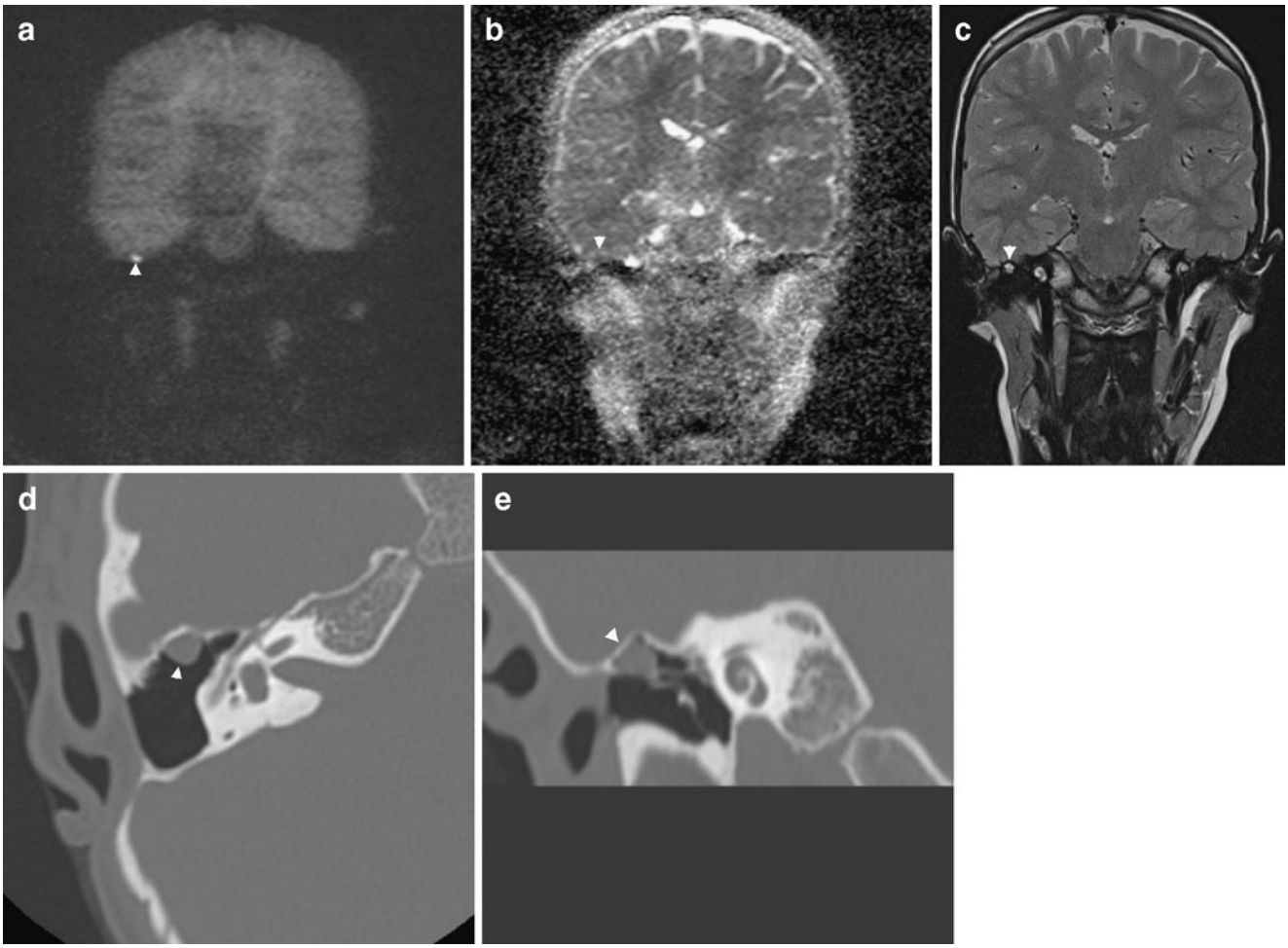

Fig. 9 A 22-year-old-male with a history of cholesteatoma on the right side treated with canal wall up tympanoplasty 3 years before. At otoscopy, a whitish lesion was suspected at the upper limit of the tympanic membrane graft. Upon these clinical and otoscopical findings, MRI—using the non-EP DW protocol—was performed first. CT scanning was performed subsequently, based upon the MR findings. **a** The coronal non-EP DW b1000 image (SS TSE DW sequence or HASTE DW sequence) clearly shows a small nodular hyperintensity (*arrowhead*) immediately beneath the right temporal lobe. **b** On the coronal ADC map (same slice position as **a**), the lesion can be seen as a small nodular hypointensity (*arrowhead*) immediately beneath the right temporal lobe. **c** Coronal 2-mm-thick TSE T2-weighted image at the level of the cochlea (same level as **a** and **b**). The lesion is seen as a small nodule with moderate and high signal intensities (*arrowhead*). **d** Axial preoperative CT image, at the level of the vestibule, shows the small nodular soft tissue density (*arrowhead*) anterior in the post canal wall up tympanoplasty cavity. **e** Coronal preoperative reformatted CT image, at the level of the cochlea. A small nodular density is found at the superior insertion of the tympanic membrane graft (*arrowhead*). Conclusion: Otoscopically, recurrent cholesteatoma at the insertion of the tympanic membrane graft was suspected. Non-EP DW imaging (b1000 images) confirmed the presence of a small recurrent cholesteatoma. Standard TSE T2-weighted sequences revealed the recurrent cholesteatoma situated anterior and superior in the temporal bone. Prior to surgery, an axial volume CT scan with coronal reformations was performed, confirming the location of the recurrent cholesteatoma at the superior insertion of the tympanic membrane graft

Extension towards the medial wall of the middle ear will erode most frequently the bony layer over the lateral semicircular canal with—in case of invasion—a possible secondary labyrinthitis in a limited number of cases (Fig. 4). The tympanic segment of the facial nerve canal can also be eroded with subsequent facial nerve palsy.

A less frequent type of cholesteatoma that can be found is the pars tensa cholesteatoma. These cholesteatomas originate from the mesotympanic part of the tympanic membrane and grow medially and upwards medial to the ossicular chain, displacing the ossicular chain laterally [8, 9].

Surgery of a pars flaccida cholesteatoma is most frequently performed using a canal wall up tympanoplasty (CWU), in which a mastoidectomy is performed, the wall of the external auditory canal is preserved, and disease is eradicated from the middle ear and mastoid. This technique, however, carries the risk of leaving cholesteatomatous tissue behind and makes clinical follow-up difficult as the intact external auditory canal does not allow inspection of the antrum and mastoid [10].

For this reason, about 1 year after first-stage surgery, a second look surgery is performed to evaluate the presence

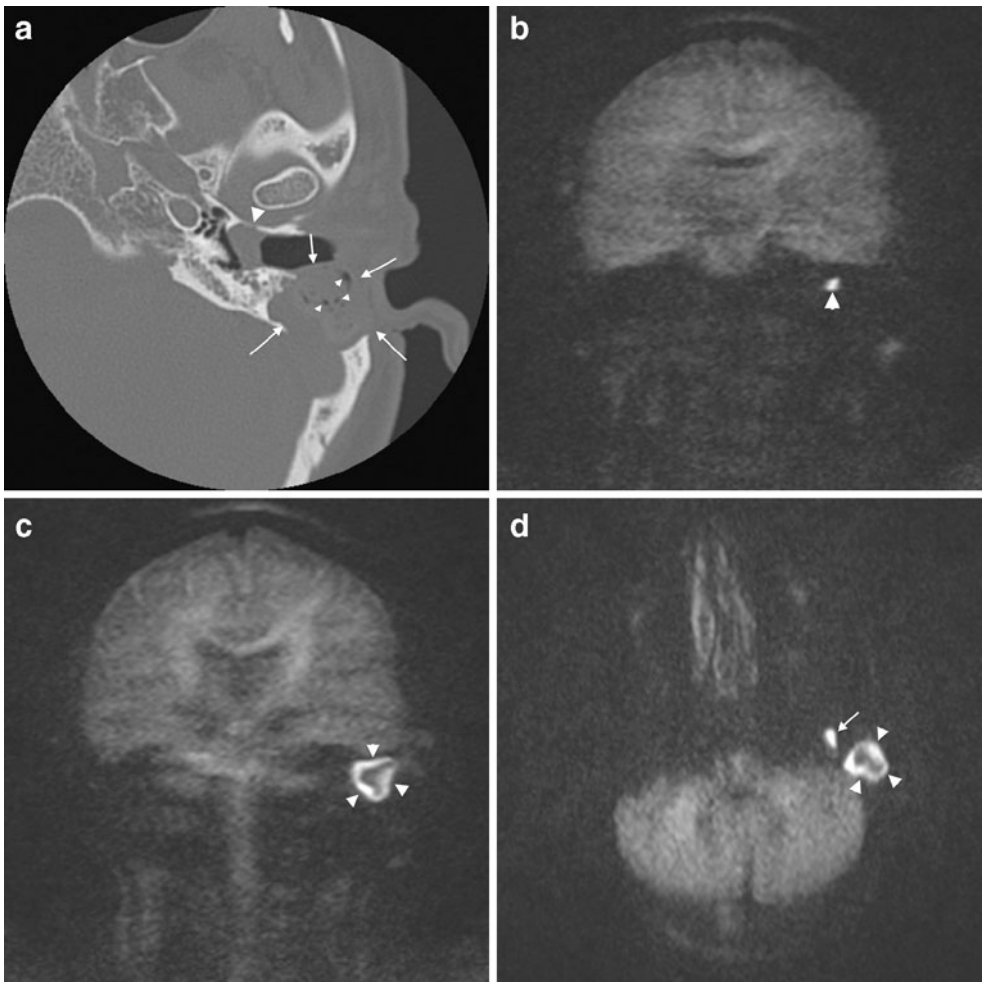

Fig. 10 A 25-year-old male with a history of canal wall up tympanoplasty at the left side for cholesteatoma 5 years before now presents with persistent ear discharge and pain. **a** Axial CT scan of the left ear presenting some soft tissue density in the external auditory canal (*large arrowhead*) and a large nodular soft tissue density (*arrows*) in the cavity created by the canal wall up tympanoplasty. Some hypodensities are noted in this soft tissue density (*small arrowheads*) and are probably presenting air. Based on CT, an abscess in the tympanoplasty cavity cannot be excluded. **b** Coronal non-EP DW b1000 image (SS TSE DW sequence or HASTE DW sequence) (at the level of the external auditory canal) shows a nodular hyperintensity (*arrowhead*) compatible with a recurrent cholesteatoma. **c** Coronal non-EP DW b1000 image (SS TSE DW sequence or HASTE DW sequence). Image (see also the position of the brain stem compared to **b**) located posterior to **b**. A large peripherally hyperintense nodular structure can be seen in the tympanoplasty cavity (*arrowheads*). **d** Axial non-EP DW b1000 image (SS TSE DW sequence or HASTE DW sequence). Both the lesions in the external auditory canal (*arrow*) and the lesion in the tympanoplasty cavity (*arrowheads*) which were visible on CT (see image **a**) have a high signal intensity. Conclusion: Both soft tissue densities on CT display a high signal intensity on the b1000 images. At surgery, cholesteatoma was found against the tympanic membrane as well as in the tympanoplasty cavity. In the tympanoplasty cavity, at surgery, the cholesteatoma demonstrated a centrally located so-called dry cholesteatoma. No abscess could be found

of a "residual" cholesteatoma. This second look surgery is performed in about 60% to 65% of patients with a higher percentage of second look surgery in children, reaching 80% [11]. The percentage of residual cholesteatoma found at second look surgery in adults is about 10% to 15%. In children, the percentage of residual cholesteatoma is higher varying between 23% and 44%, with recurrent cholesteatoma around 20% [11].

In order to lower the residual and recurrent rates of cholesteatoma in CWU techniques, primary bony obliteration techniques (PBOT) have been developed. This technique can be used during primary cholesteatoma surgery in order to treat middle ear and mastoid cholesteatoma but can also be assessed in revision cases of recurrent cholesteatoma. When using this technique, the canal wall up tympanoplasty cavity is subsequently filled up with a mixture of bone and bone pâté in order to diminish the number of recurrence through new retractions of the tympanic membrane [12–14]. A functional ossicular chain reconstruction is performed either in the same stage or in a second stage.

The number of residual cholesteatomas (15%) is lower than in the CWU technique with a recurrence rate of about 2% [14, 15].

Cholesteatoma: diffusion-weighted magnetic resonance imaging

Introduction

Evaluation of an acquired middle ear cholesteatoma was mainly done using CT scan. CT nicely demonstrates the erosion of the lateral epitympanic wall and ossicular chain. Erosion of the lateral semicircular canal can also be evaluated using CT scan [8, 9].

To see the direct effect of an associated invasion in the membranous labyrinth, MRI including T2-weighted images and post-gadolinium (Gd) T1-weighted sequences are required. On 3D heavily T2-weighted sequences, the fluid content and signal intensity of the membranous labyrinth can be evaluated. On post-Gd T1-weighted sequences, the enhancement of the membranous labyrinth should be looked after. Most frequently, it is the associated inflammation invading the membranous labyrinth and not the cholesteatoma itself that is causing enhancement (Fig. 4).

It was already noted in early reports that differentiation between inflammation and cholesteatoma is possible using Gd-enhanced T1-weighted images as cholesteatoma is by

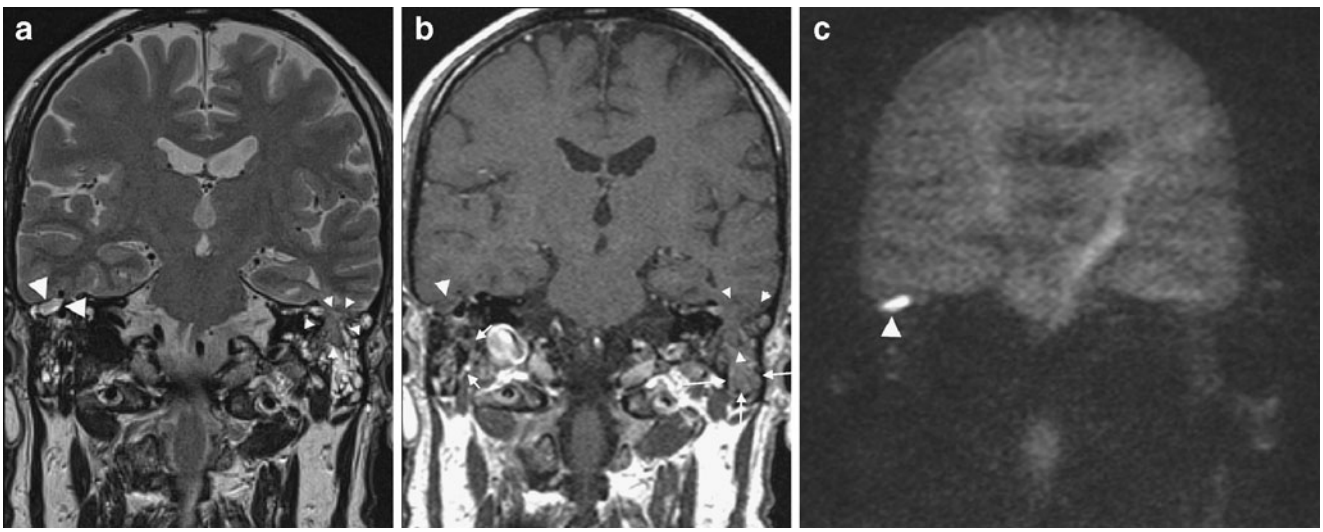

Fig. 11 A 25-year-old female with a history of cholesteatoma surgery on the left side. The clinical examination was unremarkable. **a** Coronal 2-mm-thick TSE T2-weighted MR image at the level of the mastoid. On the left side, there seems to be protrusion of a part of the temporal lobe through a defect in the tegmen (*small arrowheads*) into the mastoid. On the right side, an oval structure with intermediate signal intensity is seen beneath the tegmen (*large arrowheads*). **b** Coronal 2-mm-thick delayed post-gadolinium SE T1-weighted MR image (same level as **a**). On the left side, the protruding temporal lobe can be seen as a lesion which is isointense to brain (*small arrowheads*) and which is surrounded by enhancing inflammatory tissue with a slightly higher signal intensity (*long arrows*). On the right side, there is an oval hypointensity underneath the tegmen (*large arrowhead*), surrounded by enhancing inflammatory tissue with a clear hyperintensity (*short arrows*). **c** Coronal non-EP DW b1000 image (SS TSE DW sequence or HASTE DW sequence). The lesion on the right side demonstrates a clear high signal intensity on the non-EP DW b1000 image (*large arrowhead*). The herniated temporal lobe is not hyperintense. The intensity on the left side is comparable to the intensity of the rest of the left temporal lobe. Conclusion: On the left side, standard MR sequences are highly suspicious of a herniated left temporal lobe. On the right side, by surprise, an attical cholesteatoma was found. Both findings were confirmed by surgery

definition "avascular tissue" and does not enhance in contrast to inflammation which clearly enhances [16].

Fitzek was one of the first to demonstrate the hyperintense aspect of cholesteatoma on b1000 EP DW images. This hyperintense aspect was completely different from the complete lack of hyperintensity of middle ear inflammatory changes on b1000 EP DW images [17]. Major drawbacks of the EP DW sequences are, however, the low resolution, the rather thick slices, and the susceptibility artefacts at the interface temporal lobe and temporal bone limiting clearly the capability of this sequence to detect smaller cholesteatomas [18].

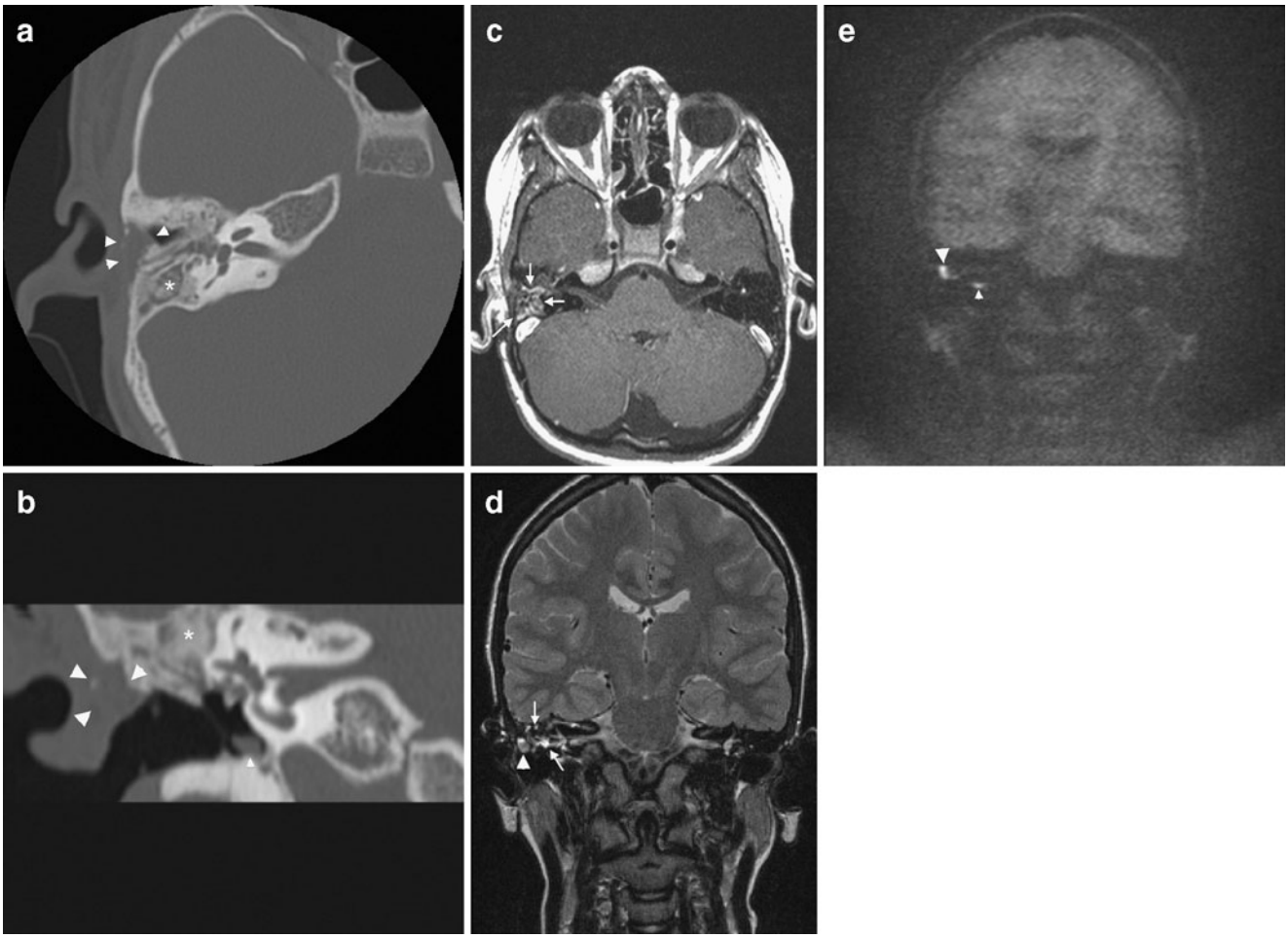

Fig. 12 An 18-year-old male operated for a cholesteatoma on the right side using the primary bony obliteration technique (PBOT) or technique of Mercke. In this technique, the cavity created by the canal wall up (CWU) technique is filled up with a mixture of bone and bone pâté. The obliteration of the resection cavity results in a much lower incidence of cholesteatoma recurrence compared to the classical CWU technique. **a** Axial CT scan at the level of the oval window and vestibule. The CWU tympanoplasty cavity is filled up using material with both soft tissue and bone density (*asterisk*). There are some soft tissues left at its anterior and lateral border (*arrowheads*). **b** Coronal reformatted CT image at the level of the oval window and internal auditory canal. The CWU tympanoplasty cavity is filled up using a mixture of bone and bone pâté (*asterisk*). Note that there are some soft tissues left in the hypotympanum (*small arrowheads*) and lateral and caudal to the cavity (*large arrowheads*). **c** Axial delayed post-gadolinium T1-weighted image at the level of the vestibule and internal auditory canal (same level as **a**). The signal intensities of the PBOT are mixed and inhomogeneous (*arrows*). Due to the mixed character of these signal intensities, it is impossible to detect the characteristic signal intensities of a residual cholesteatoma. No conclusions can be drawn from this sequence. **d** Coronal TSE T2-weighted image at the level of the vestibule and internal auditory canal (same level as **b**). The signal intensities of the PBOT are mixed and inhomogeneous (*arrows*). There are several small regions of very low signal intensity probably due to signal void of small parts of bone. Note a nodular zone of intermediate signal intensity (*arrowhead*). **e** Coronal non-EP DW b1000 image (SS TSE DW sequence or HASTE DW sequence) (same level as **b** and **d**). There are two small regions of clear hyperintensity (*small and large arrowheads*). Correlation with **b** and **d** shows that there is residual cholesteatoma in the hypotympanum and lateral to the obliterated cavity (see also the nodular zone of intermediate intensity on **d**). Conclusion: Diffusion-weighted MRI reveals two nodules of residual cholesteatoma situated in the hypotympanum and lateral to the obliterated cavity. Diagnosis can only be reliably made based upon the non-EP DW images. Correlation with CT makes it possible to localize the lesions. It is striking that in case of PBOT, the residual or relapsing cholesteatoma is usually found at the periphery of the obliteration but never in the center of the obliteration

Recent papers have highlighted the advantages of non-echoplanar-based diffusion-weighted sequences. These sequences are most frequently single shot or multishot-based turbo spin echo diffusion-weighted sequences. They have a thinner slice thickness, a slightly higher resolution, and a complete lack of artefacts compared to echo planar diffusion-weighted sequences [3].

Congenital cholesteatoma

The congenital cholesteatoma situated in the middle ear is very difficult to evaluate clinically.

The presence of a congenital middle ear cholesteatoma is often suspected in the presence of a whitish lesion behind an intact tympanic membrane on otoscopic evaluation. Most oftenly, a conductive hearing loss is discovered. Congenital cholesteatomas are most frequently detected during childhood.

CT, however, is able to nicely demonstrate the nodular soft tissue lesion located very often in the middle ear around the ossicular chain. The intact tympanic membrane and the nodular soft tissue mass lesion in a young patient on an atypical location must attract the attention of the radiologist towards the diagnosis of a congenital cholesteatoma.

Due to the fact that congenital middle ear cholesteatomas are very often small lesions, EP DW MRI is unable to detect and characterize congenital middle ear cholesteatoma [18]. Non-EP DW MRI, however, is able to detect and characterize the congenital middle ear cholesteatoma due to its thinner slice thickness, higher resolution, and lack of artefacts. It nicely shows the very small nodular hyperintensity on b1000 images.

Even a congenital cholesteatoma as small as 2 mm can be detected and characterized on non-EP DW MRI [19] (Fig. 1). Moreover, correlation with apparent diffusion coefficient (ADC) maps nicely shows the hypointensity of the congenital cholesteatoma caused by the diffusion restriction in the cholesteatoma.

In case of congenital cholesteatoma situated in the petrous bone near or in the membranous labyrinth, the use of CT and MRI is mandatory. CT is needed to demonstrate the sharply delineated punched-out soft tissue lesion and to show the relation to the geniculate ganglion and the structures of the membranous labyrinth. On DW MRI, the diagnosis is straightforward showing the clear hyperintensity of the lesion on b1000 images. On EP DWI, the lesions look rather distorted, while congenital cholesteatoma shows a sharply delineated, nodular hyperintense aspect on non-EP DWI. It is even helpful in the description of the extension by clearly showing the hyperintensity of the congenital cholesteatoma (Fig. 2).

Even though the diagnosis can be made on DW MRI images, correlation with standard TSE T2-weighted images, 3D thin slice heavily T2-weighted images, and thin slice post-Gd T1-weighted is complementary in the description of the exact extension and invasion in the different structures of the membranous labyrinth.

Differential diagnosis with other lytic lesions in or around the membranous labyrinth can be made based upon the location and aspect of the lesion, its delineation, and the signal intensity on b1000 diffusion-weighted images. Congenital cholesteatoma is the only lesion showing a frank hyperintensity on b1000 diffusion-weighted images. Endolymphatic sac tumor and glomus jugulo-tympanicum have a rather specific predilection site. Endolymphatic sac tumor displays mixed signal intensities on standard MRI sequences with enhancement. Glomus jugulo-tympanicum has, apart from its specific predilection site and strong enhancement with salt and pepper appearance on standard sequences, a characteristic MR angiographic appearance. On unenhanced 3D TOF MR angio, the high signal intensity of the small intralesional vessels can be seen. On CT, it shows a very irregular permeative lytic bone pattern. Metastatic lesions to the temporal bone also have a very irregular lytic aspect compared to the sharply delineated and regular lytic aspect of congenital cholesteatoma. Metastatic lesions also enhance.

The facial nerve schwannoma also has a predilection site for the geniculate ganglion, but it follows the course of the facial nerve whereas the congenital schwannoma extends beyond the limits of the facial nerve course. Moreover, the facial nerve schwannoma always enhances. Hemangiomas located in the geniculate ganglion region limit themselves to the region of the geniculate ganglion but also display characteristic calcifications on CT. Moreover, both facial

Table 1 Signal intensity on various sequences of the most frequent lesions and pseudolesions of the apex of the petrous bone.

	T1 WI	T2 WI	b1000 DW	ADC map
Asymmetric apex air	Signal void	Signal void	No signal	No signal
Asymmetric apex fat	Very high	Moderately high	Low	High
Opacified/infected apex	Low	High	Low	High
Cholesterol granuloma	High	High	Moderately high	High
Cholesteatoma	Low	High	High	Low
Petrous apex cephalocele	Low	High	Low	High

nerve schwannomas and hemangiomas do not display any hyperintense signal on b1000 DW MRI.

A non-EP DW MRI sequence should definitely be included in the MR evaluation of a middle ear soft tissue lesion and in the evaluation of a lytic lesion in the temporal bone pyramid.

Acquired middle ear cholesteatoma

Introduction In the past few years, the role of diffusion-weighted MRI in the evaluation of patients with acquired middle ear cholesteatoma has increasingly grown.

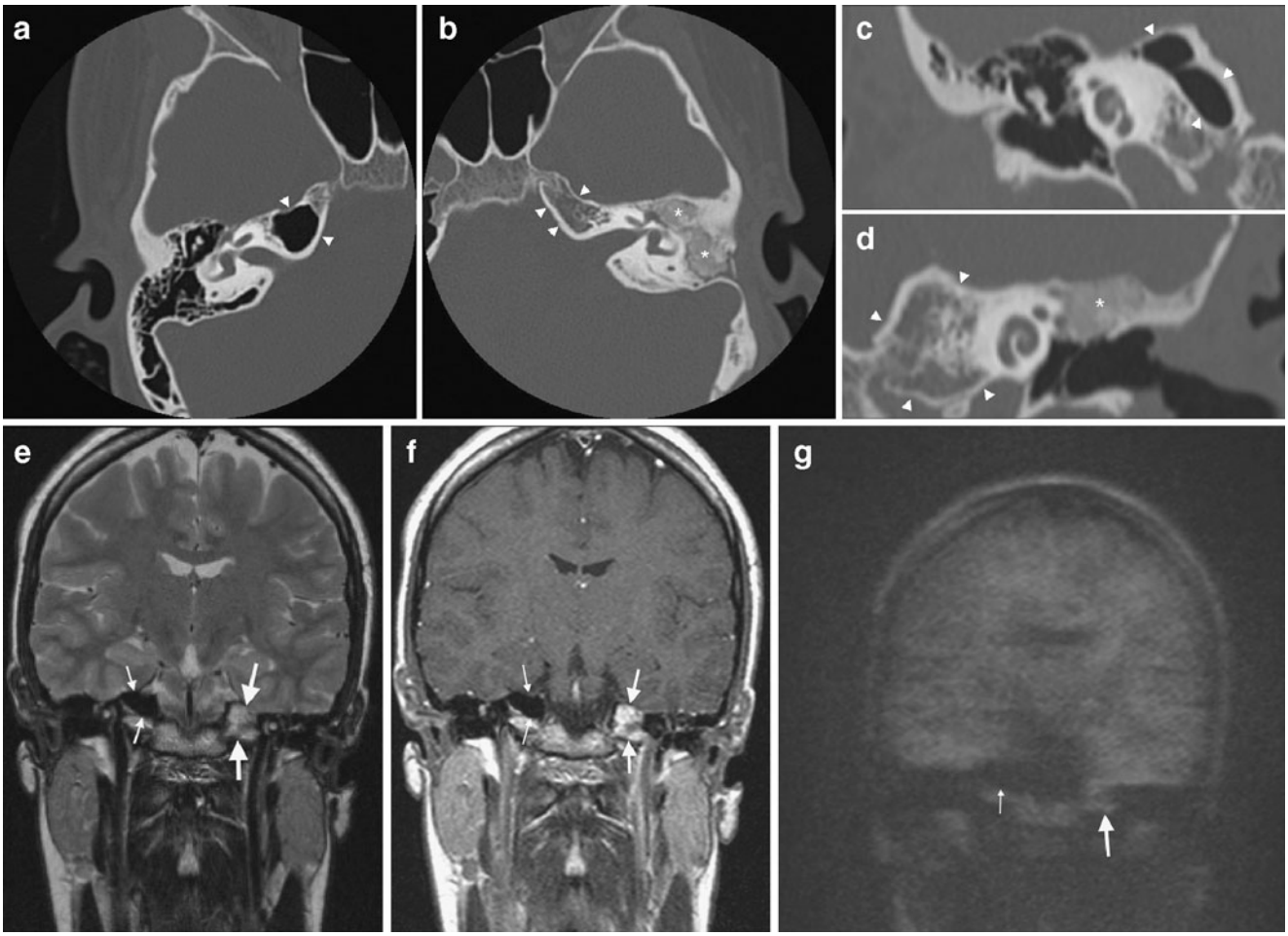

Fig. 13 A 16-year-old female with a history surgery for left-sided middle ear cholesteatoma. A primary bony obliteration technique was performed. **a** Right-sided axial CT scan at the level of the tympanic segment of the facial nerve. There is a clear aeration of the apex of the right petrous bone (*arrowheads*). **b** Left-sided axial CT scan at the level of the tympanic segment of the facial nerve (same level as **a**). There is a non-aerated apex of the left petrous bone (*arrowheads*). Note the PBOT technique in the left mastoid in which the entire mastoid is filled with a mixture of bone and bone paté, obliterating the entire mastoid and epitympanum (*asterisks*). **c** Coronal CT reformation at the level of the cochlea. There is a clear aeration of the apex of the right petrous bone (*arrowheads*). **d** Coronal CT reformation on the left side (same level as **c**). Note the lack of aeration (*arrowheads*) and the obliterated aspect of the epitympanum (*asterisk*). **e** Coronal 2-mm TSE T2-weighted image (same level as **c** and **d**). Asymmetry at the level of the apex of petrous bone. The hypointensity on the right side is explained by the presence of air in the aerated apex (*small arrows*). The hyperintensity on the left side is explained by the presence of fat containing bone marrow in the apex of the left petrous bone apex (*large arrows*). **f** Coronal post-gadolinium SE T1-weighted image (same level as **c**, **d**, and **e**). Note again the hypointensity—caused by air—in the apex of the right petrous bone (*small arrows*). The left-sided hyperintensity is explained by the presence of fat (*large arrows*). **g** Coronal non-EP DW image (SS TSE DW sequence or HASTE DW sequence) (same level as **c**–**f**). The asymmetry is also visible on this b1000 image in which the air-filled apex of the right petrous bone displays a marked hypointensity (*small arrows*) and the left fat filled apex of the petrous bone has an intermediate to low signal intensity (*large arrows*). Conclusion: Clear asymmetry in the apex of the petrous bone explained by the air in the apex of the petrous bone on the right side and the fatty bone marrow on the left side. CT is straightforward in diagnosing this asymmetry but signal intensities on MRI can be confusing, especially when correlation with CT is not available. This asymmetry is one of the major causes of a "pseudo-tumoral" lesion of the petrous bone apex on MRI. In the MRI differential diagnosis, one should include cholesterol granuloma, but this entity displays a definite higher signal intensity on T2-weighted images. Petrous apex cholesteatoma is excluded due to the lack of hyperintensity on b1000 DW images and due to the hyperintense aspect of the lesion on T1-weighted images

In the evaluation of middle ear cholesteatoma, non-EP DW imaging has the advantage over EP DW imaging regarding thinner slices, a higher resolution, and a complete lack of artefacts [3]. Non-EP DW imaging is able to detect cholesteatoma as small as 2 mm in size whereas this is limited to 5 mm for EP DW imaging [18, 19]. In the evaluation of acquired middle ear cholesteatoma, preference should definitely be given to non-EP DW sequences over EP DW sequences.

Acquired middle ear cholesteatoma In case of a clinical and otoscopical straightforward cholesteatoma, imaging evaluation prior to first stage surgery is done by CT, showing the erosive changes to the lateral epitympanic wall and the ossicular chain [8, 20, 21]. In case of a clinical and/or otoscopical unequivocal diagnosis of a cholesteatoma, detection and diagnosis of a middle ear cholesteatoma can be performed using non-EP DW sequences as a screening tool. In order to localize the cholesteatoma, axial and

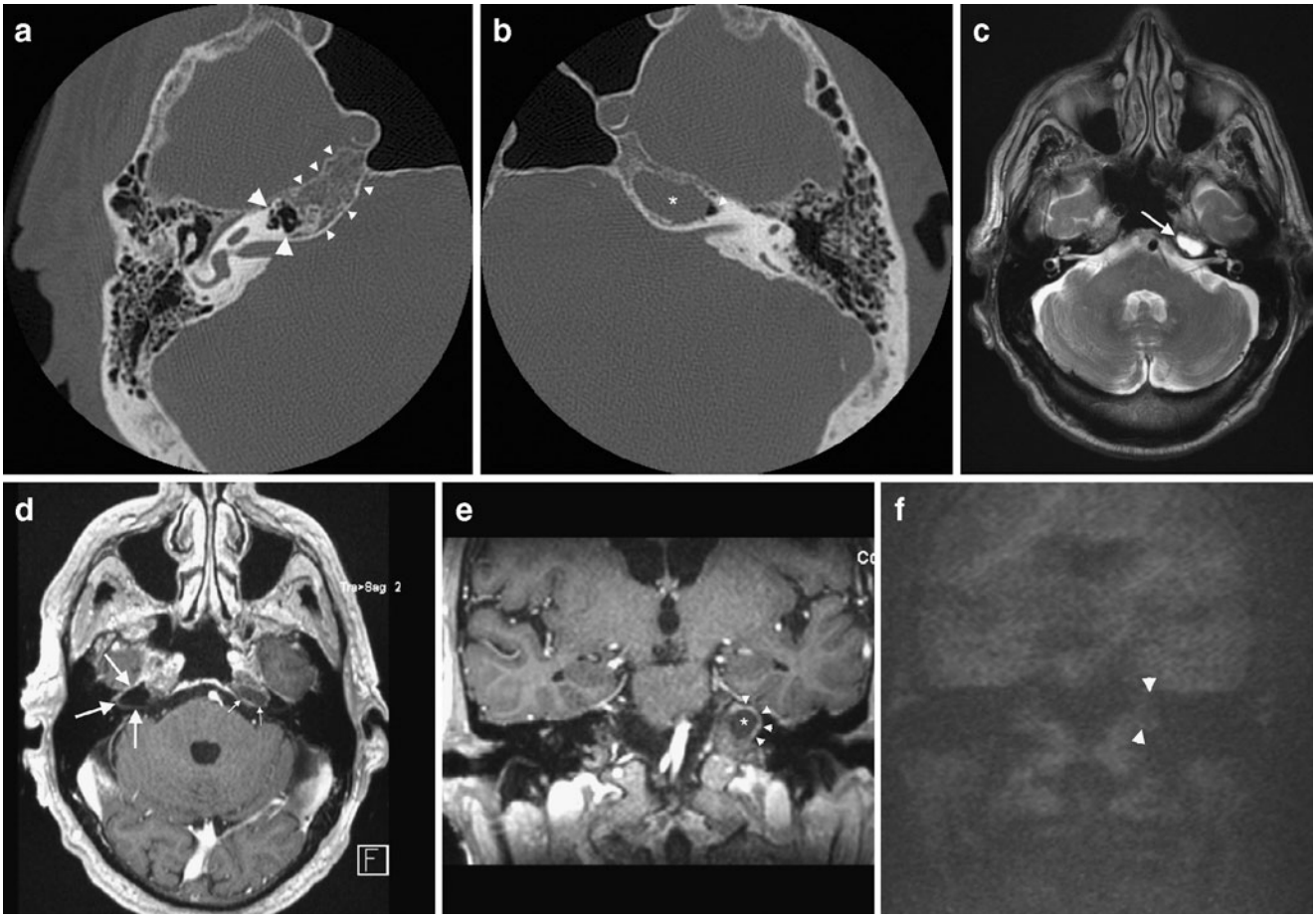

Fig. 14 A 39-year-old female presenting with mixed hearing loss on the right side. **a** Axial CT scan of the right temporal bone at the level of the vestibule, maleus head, and incus body. A well aerated middle ear and mastoid can be noted. There is aeration of the petrous bone medially to the otic capsule (*large arrowhead*). Note the homogeneous ossification of the petrous apex (*small arrowheads*). **b** Axial CT scan of the left temporal bone at the level of the superior semicircular canal. Note the homogeneous nodular density in the apex of the petrous bone (*asterisk*). There is a small triangular air density posterior to it (*small arrowhead*). This small air density is suggestive of a near total opacified aerated petrous apex with fluid and/or inflammation. **c** Axial 4-mm-thick TSE T2-weighted image through the posterior fossa at the level of the internal auditory canal. There is a nodular hyperintense lesion in the apex of the left petrous bone (*arrow*). Note that the lesion has a slightly higher intensity than CSF. **d** Axial 2-mm-thick post-gadolinium SE T1-weighted image at the level of the internal auditory canal. The lesion situated in the apex of the left petrous bone (*small arrows*) shows a central hypointensity with a linear peripheral enhancement. Note the homogeneous hypointense petrous bone apex on the right side (*large arrows*). **e** Coronal 2-mm-thick post-gadolinium SE T1-weighted image at the level of the cochlea. The lesion has a central hypointensity (*asterisk*). Note the peripheral enhancement (*arrowheads*). **f** Coronal 2-mm non-EP DW MR b1000 image (Singe Shot (SS) TSE DW sequence or HASTE DW sequence) (same level as **e**). The lesion can be suspected on this b1000 images but displays a complete lack of hyperintensity (*arrowheads*). Conclusion: The most likely diagnosis on CT scan is an opacified apex cell of the left petrous bone. Standard MR sequences exclude the diagnosis of a petrous apex cholesterol granuloma as the lesions display no hyperintensity on T1-weighted images. A petrous bone apex cholesteatoma is excluded on the b1000 diffusion-weighted images and can be recognized by the complete lack of hyperintensity. The final diagnosis is an opacified and inflammed petrous apex. Eventually, this lesion might evolve into a petrous apex mucocele

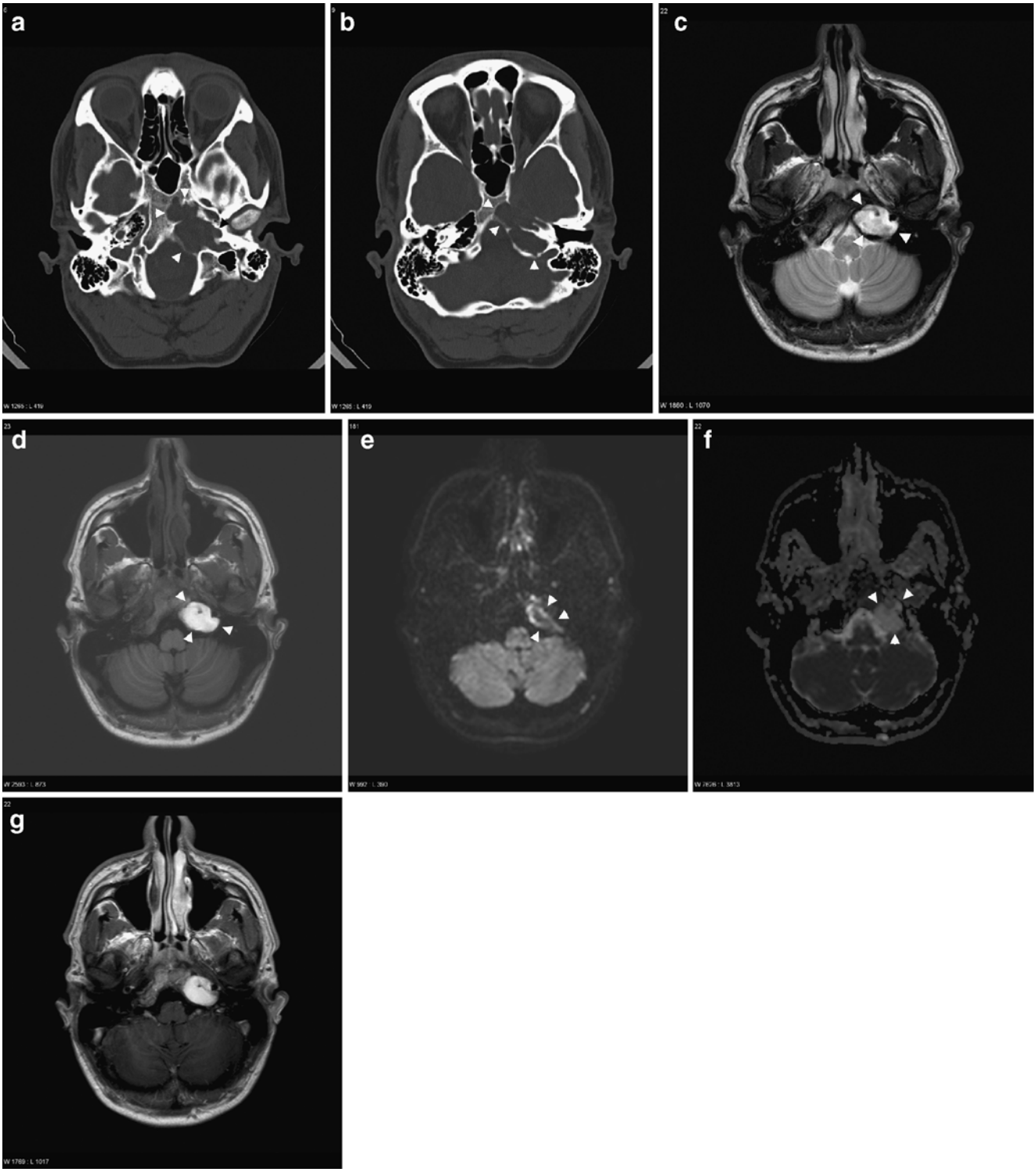

coronal TSE T2-weighted sequences are added. Gadolinium administration is—in those cases—not required [22].

However, in case of clinical suspicion of associated infection and/or inflammation, the combination of non-EP DW sequences and delayed post-Gd T1-weighted and TSE T2-weighted sequences will be able to differentiate the cholesteatoma from the surrounding infection or inflammation. In case of an associated complication, the combination of standard sequences after gadolinium administration and non-EP DW sequences is recommended (Fig. 4).

There are two reasons for false-negative examinations on DW sequences. Evacuation of the keratin from the

◀ **Fig. 15** A 32-year-old male presenting with headache. **a** Axial CT image (bone window) through the skull base at the level of the clivus. A sharply delineated lytic lesion is seen in the skull base and clivus on the left side (*arrowheads*). **b** Axial CT image (bone window) through the skull base at the level of the petrous apex demonstrating a large sharply delineated lytic lesion (*arrowheads*). **c** Axial 3-mm-thick TSE T2-weighted MR image through the posterior fossa. The lesion has a homogeneous hyperintense appearance (*arrowheads*). **d** Axial 3-mm-thick SE T1-weighted MR image through the posterior fossa. The lesion displays a homogeneous hyperintense signal (*arrowheads*). **e** Axial 3-mm-thick EP DW MR image through the posterior fossa. The lesion remains hypointense (*arrowheads*). **f** Axial ADC map. Note the hyperintense aspect of the lesion on the ADC map. The lesion has no diffusion restriction. **g** Axial post-gadolinium 3-mm-thick SE T1-weighted MR image. The lesion is not enhancing. Conclusion: Large, sharply delineated lesion in the apex of the left petrous bone, with spontaneous hyperintensity on T2- and T1-weighted images, without any hyperintensity on b1000 diffusion-weighted images or diffusion restriction on ADC map, compatible with a large cholesterol granuloma of the petrous apex (Courtesy of T. Stadnik, T. Buisseret UZ Brussel, Jette, Belgium)

cholesteatoma sac—by auto-evacuation or suction cleaning—will cause a false-negative examination as DW sequences detect the keratin inside the cholesteatoma (Fig. 5) [17–19]. Those cholesteatomas are also called "mural" cholesteatomas [9]. They form the major subgroup of false-negative DW examinations. Delineation of such an evacuated cholesteatoma is difficult even on standard MR sequences after gadolinium. Theoretically, one should be able to delineate the cholesteatoma matrix or epithelium on post-Gd T1-weighted sequences, but this remains very difficult due to the often surrounding inflammation (Fig. 5).

Motion artefacts degraded examinations will also result in a false-negative examination as in these cases the signal intensities of small cholesteatomas on b1000 non-EP DW sequences get smeared out over multiple pixels [19]. This should be taken into consideration especially in the pediatric population.

False-positive results on DW sequences are rare. There have been reports of false-positive results in cases with acute middle ear infection [17], bone powder [4], silastic sheets [23], granulation tissue [23], and scar tissue [24].

From our own experience, we know that accumulation of cerum in the external auditory canal can give a hyperintense signal on DW sequences. Correlation with standard TSE T2-weighted sequences nicely depicts the cerum in the external auditory canal (Fig. 6). Accumulated sebum in a sebum cyst also gives rise to a hyperintense signal. Careful interpretation of the images will show that the lesion is situated outside the temporal bone (Fig. 7).

Pre-second look evaluation One of the greatest challenges in the past decade has been the question whether MRI could replace second look surgery and if patient selection for second look surgery is possible using MRI.

First and foremost, differentiation should be made between residual and recurrent cholesteatoma [25, 26]. Residual cholesteatomas are cholesteatomatous pearls left behind at first-stage surgery. It is known that the use of CWU tympanoplasty implies a high number of residual cholesteatomas. They can be found anywhere in the middle ear or mastoid cavity and are usually rather small at the time of detection. Due to this small size and the fact that they can be found anywhere in the middle ear and mastoid cavity, they are difficult to detect (Fig. 8).

Recurrent cholesteatoma is cholesteatoma originating again in a retraction pocket at the tympanic membrane or tympanic membrane graft (Fig. 9). Recurrent cholesteatoma takes more time to develop and is usually larger at the time of detection (Fig. 10).

Early reports on the value of standard MRI sequences replacing second look surgery were very disappointing [27]. However, in the last decade, two major types of MR protocols have emerged in the evaluation of cholesteatoma patients prior to second look.

Delayed post-Gd T1-weighted sequences have been reported to be able to detect residual cholesteatoma prior to second look as small as 3 mm. The rationale is based upon the fact that postoperative changes take time to enhance. Therefore, immediate post-Gd T1-weighted imaging can result in a false-positive finding of cholesteatoma. In literature, using this protocol, patients usually get preselected based upon CT findings [28, 29].

Echoplanar diffusion-weighted imaging has various reported sensitivities ranging from 12.5% to 86% [18, 23, 24, 30, 31]. Specificity varies from 73% to 100% [18, 23, 24, 30, 31].

This is explained by the fact that in some studies residual cholesteatomas [18, 23] were evaluated, and in other studies, a mixture of residual and recurrent cholesteatomas was used [24, 30, 31]. EP DW studies have a reported size limit of 5 mm. This is the main reason why EP DW sequences are unable to detect residual cholesteatomas and cannot replace second look surgery [18].

Using EP DW sequences, very high positive predictive values (PPV) were reported (between 80% and 100%), meaning that a positive diagnosis of a cholesteatoma can be made if a hyperintense lesion is detected, provided that artefacts are not misinterpreted as a cholesteatoma [18, 23, 24, 30, 31]. Negative predictive values (NPV) are reported to be variable (between 40% and 75%). This is explained by the fact that—due to size limits—a lot of false-negative cases are reported.

However, non-EP DW sequences have been reported to be able to replace second look surgery. Using the combination of non-EP DW sequences and delayed post-Gd sequences, a sensitivity of 90% and a specificity of 100% can be achieved [32]. One Australian group even

screens patients prior to second look using non-EP DW sequences alone [33, 34].

Recent literature has indeed demonstrated that non-EP DW sequences alone have the same sensitivity, specificity, PPV, and NPV than the combination of non-EP DW sequences and delayed post-Gd T1-weighted sequences together. Non-EP DW sequences have also a significantly higher sensitivity, specificity, PPV, and NPV than delayed post-Gd T1-weighted sequences [22].

Therefore, evaluation of cholesteatoma patients can be performed prior to second look surgery using non-EP DW sequences alone [22, 33, 34]. In order to be able to localize suspected lesions on the non-EP DW sequences, an axial and coronal TSE T2-weighted sequence is added [22].

Cholesteatoma patients should definitely be selected for second look surgery using non-EP DW sequences (Fig. 8) [22, 33, 34]. CT scanning should no longer be used as the first imaging tool prior to second look surgery. CT scanning prior to second look should only be used in case of a positive MR examination using non-EP DW sequences in an immediate presurgical setting. This will inevitably reduce the number of useless irradiated patients prior to second look surgery.

MRI, including DW sequences, is extremely useful in the evaluation of possible postoperative complications.

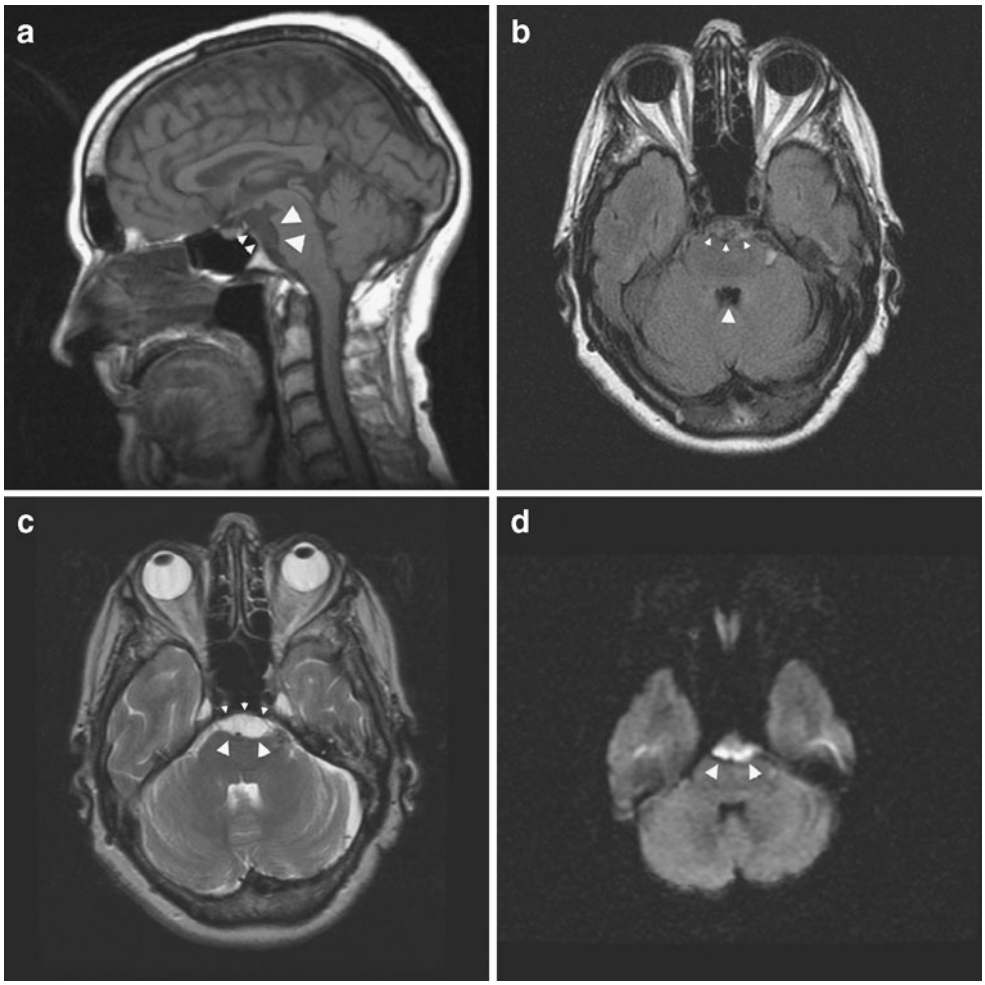

Fig. 16 A 72-year-old male presenting with headache. **a** Sagittal 3-mm-thick SE T1-weighted image. A slightly inhomogeneous mass lesion is seen in the prepontine cistern (*small arrowheads*) with compression on the brain stem (*large arrowheads*). The linear flow void situated just anterior to the brain stem is the compressed basilar artery. **b** Axial 3-mm-thick FLAIR image through the posterior fossa. The mass lesion demonstrates an inhomogeneous appearance (*small arrowheads*). Compare with the homogeneous hypointense appearance of the CSF in the fourth ventricle (*large arrowhead*). **c** Axial 3-mm-thick TSE T2-weighted image through the posterior fossa. The mass lesion has a homogeneous high signal intensity (*small arrowheads*) and compresses the brainstem and basilar artery (*large arrowheads*). **d** Axial 4-mm EP DW b1000 image showing the hyperintense signal intensity of the mass lesion (*arrowheads*). Conclusion: Epidermoid cyst in the prepontine cistern. Differential diagnosis with an arachnoid cyst cannot be made based on the findings on the T2- and T1-weighted sequences. On FLAIR images, epidermoid cysts typically have an inhomogeneous appearance with an intensity higher than that of CSF. The diagnosis is confirmed on diffusion-weighted images on which the epidermoid cyst has a high signal intensity on b1000 images. Note the distorted aspect of the epidermoid cyst on this EP DW sequence

Particularly in case of an associated tegmen defect, one cannot differentiate soft tissues in the middle ear. MRI and DW sequences in particular have the possibility to differentiate associated soft tissue lesions. Meningoceles and meningoencefaloceles can easily be detected on MRI (Fig. 11).

Following a PBOT, imaging becomes even more important as there is still the risk of burying a residual cholesteatoma in the bony obliterated cavity. The rate of residual and recurrent cholesteatoma has been reported to be much lower than in the CWU technique.

EP DWI seems to be useless in the evaluation of these patients as these lesions are very small [35]. However, again, non-EP DW sequences are reported to have the highest sensitivity and specificity [36]. Recurrences are situated in most cases superficial to the obliterated mastoid or at the interface between the obliterated mastoid and the middle ear cavity (Fig. 12). In these cases, CT is complementary to MRI—using non-EP DW sequences—in showing the corresponding CT soft tissues densities to the MR reported hyperintensities (Fig. 12).

Petrous apex lesions

DW MRI is also very helpful in the differentiation of various lesions in the petrous bone apex [37, 38] (Table 1). Asymmetry in aeration of the petrous bone apex is one of the most common pseudo-tumorous lesions of the petrous

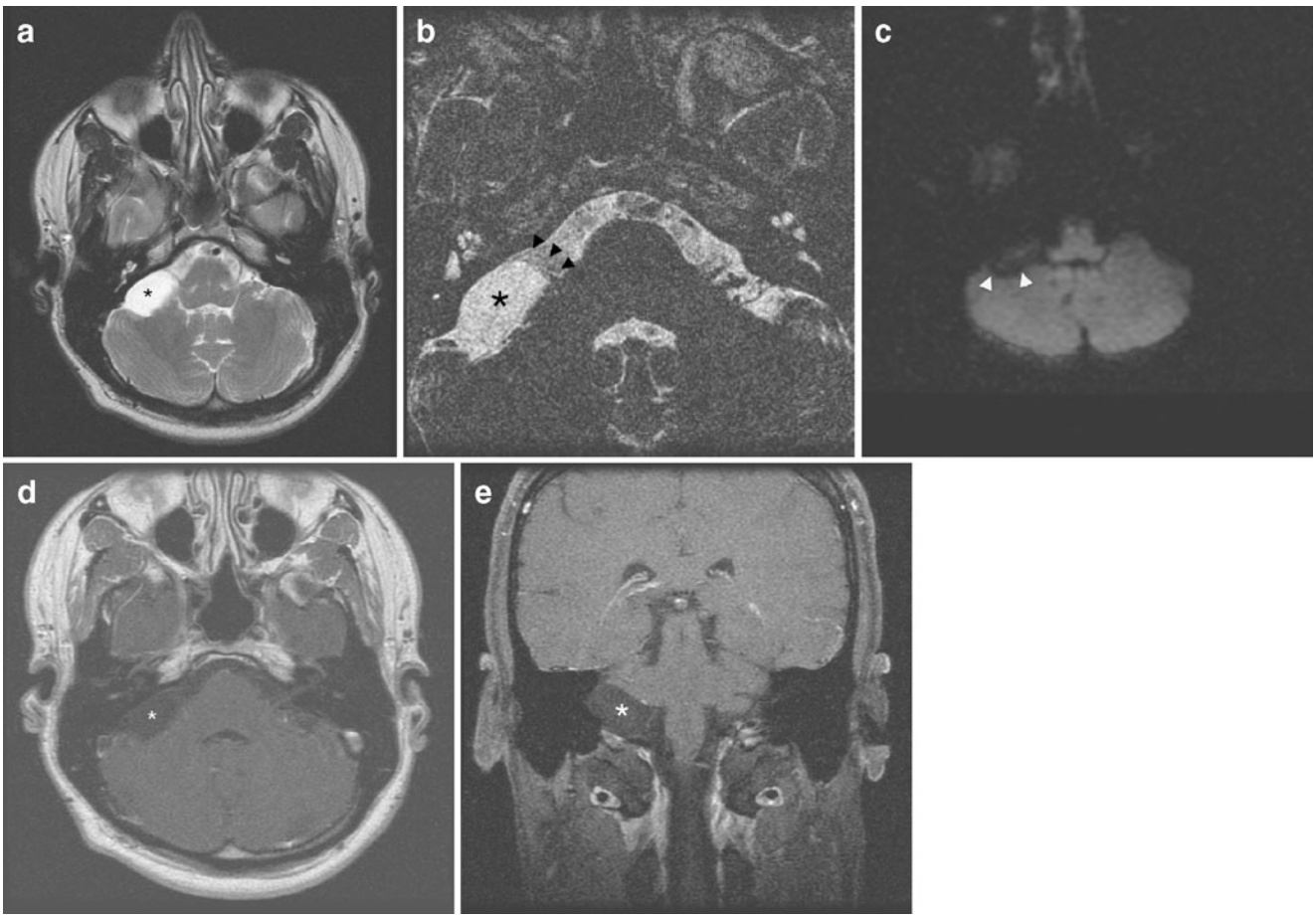

Fig. 17 A 55-year-old male investigated for sensorineural hearing loss on the left side. **a** Axial 4-mm-thick TSE T2-weighted MR image through the posterior fossa. In the posterior part of the right CPA, a nodular homogeneous hyperintense lesion is found (*asterisk*). The intensity is homogeneous and the lesion is sharply delineated. **b** Axial 1-mm-thick 3D TSE T2-weighted MR image through the posterior fossa. The lesion is situated in the posterior and lateral aspect of the right CPA, showing a homogeneous hyperintensity (*asterisk*). There is anterior displacement of the right vestibulo-cochlear and facial nerve (*arrowheads*). **c** Axial 4-mm-thick EP DW b1000 image. The lesion has a low signal intensity (*arrowheads*). **d** Axial 2-mm-thick SE T1-weighted image after gadolinium administration. There seems to be no enhancement of the homogeneous hypointense lesion (*asterisk*) in the right CPA. **e** Coronal 2-mm-thick SE T1-weighted image with fat saturation after gadolinium administration. There is a clear asymmetry with visualization of an oval homogeneous hypointense lesion in the right CPA (*asterisk*). There is no enhancement. Conclusion: The lesion has CSF-like intensities and has no high signal intensity on diffusion-weighted images. Based on these findings, diagnosis of a right-sided arachnoid cyst can be made (compare to Fig. 16)

bone apex (Fig. 13). If one apex is aerated, it displays a signal void on standard MR sequences as well as on diffusion-weighted sequences. The contralateral non-aerated apex contains fat with a high intensity on T1-weighted sequences and a moderate intensity on T2-weighted sequences. It lacks, however, a clear high intensity on b1000 DW MRI. Some hyperintensity can, however, be noted due to T2 shine through. The intensity on T2-weighted sequences is much lower that the intensity of cholesterol granuloma (see below) [37, 38].

An aerated petrous bone apex can get fluid filled and infected, displaying a low intensity on T1-weighted sequences with possible peripheral enhancement. On T2-weighted sequences, signal intensity is high. On b1000 DW MRI, there is no high signal intensity making the differential diagnosis with a petrous bone apex cholesteatoma possible (Fig. 14).

In the chronic phase, a mucocele of the petrous apex can develop areas of higher signal intensity on T1-weighted images and low signal intensity on T2-weighed images with an expansile appearance of the lesion on MRI and CT. Again, this lesion displays no hyperintensity on the b1000 diffusion-weighted sequence [37, 38].

A petrous bone apex cholesterol granuloma is the most common primary lesion of the petrous apex accounting for about 60% of all lesions in that region. They can occur bilateral. A history of serous or chronic otitis media has been identified as a major risk factor for the development of a cholesterol granuloma. They contain a brownish liquid with cholesterol crystals. Repetitive cycles of hemorrhage and granulomatous reaction initiated by an obstruction of the ventilation outlet of the apex are believed to be the cause [37, 38].

The entity of a petrous bone apex cholesterol granuloma presents as an expansile lesion with a clear high signal intensity on T1-weighted as well as on T2-weighted images (Fig. 15). This lesion does not display a high signal intensity on diffusion-weighted sequences. A slight hyperintensity can, however, be seen due to a T2 shine through effect. However, signal intensity on an ADC map remains high in contrast to the drop of signal intensity in case of a cholesteatoma. The contralateral petrous apex is usually pneumatized [37, 38].

Petrous bone apex cholesterol granuloma should be differentiated from the petrous bone apex cholesteatoma. This is again an expansile lesion with signal intensities comparable to the signal intensities of middle ear cholesteatoma: low signal intensity on T1-weighted sequences and a high signal intensity on T2-weighted sequences. To differentiate such a lesion from an opacified petrous bone apex or a petrous bone apex mucocele, diffusion-weighted MRI is very helpful and will display a clear hyperintensity on b1000 images with a drop in signal intensity on ADC map (Fig. 3).

Discussion still exists if a petrous bone apex cholesteatoma is a congenital cholesteatoma or an acquired cholesteatoma extending from the middle ear to the petrous bone apex [39]. There is a tendency towards the hypothesis

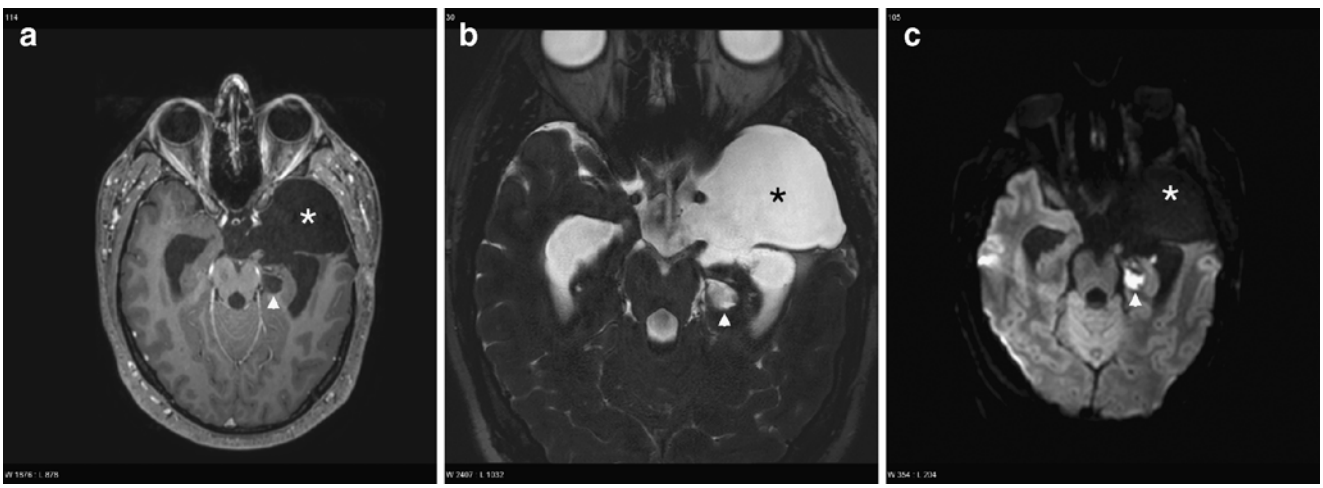

Fig. 18 A 38-year-old female with a history of surgery for a large CPA epidermoid with supratentorial extension. Imaging performed in the follow-up status of the patient. **a** Axial post-gadolinium 3D GRE T1-weighted image. There is a large hypointense region in the left temporal region probably a region of tissue loss as a postoperative sequel (*asterisk*). There is another rounded hypointense region deep in the left temporal lobe (*arrowhead*). **b** Axial 2-mm-thick MPR of a 0.4-mm 3D TSE T2-weighted sequence. Large hyperintense region in the left temporal region, probably a region of tissue loss as a postoperative sequel (*asterisk*). There is another rounded hyperintense region deep in the left temporal lobe (*arrowhead*). **c** Axial 3-mm-thick non-EP DW sequence. The large area in the left temporal fossa is indeed a postoperative sequel with an area of tissue loss (*asterisk*). However, the small nodule deep in the left temporal lobe is a remnant of the epidermoid cyst (*arrowhead*). Conclusion: Large region of postoperative tissue loss in the left temporal lobe. Diffusion-weighted imaging is, however, the only technique that is able to demonstrate or exclude a residual epidermoid cyst

that a petrous bone apex cholesteatoma is always an extension of a middle ear cholesteatoma into the petrous bone apex.

Petrous apex cephaloceles may be confused with "cystic"-like appearing lesions of the petrous apex such as the opacified petrous bone apex or the cholesteatoma. They result from herniation of the posterolateral dural wall of Meckel's cave into the anterolateral aspect of the petrous bone. It is frequently associated to a hydrops of Meckel's cave and to an empty sella. Signal intensities on standard sequences are those of cerebrospinal fluid (CSF) and the lesion shows a sharply delineated scalloping of the anterior and lateral aspect of the temporal bone [37, 38, 40]. Apart from the fact that the lesion is eccentric to the petrous bone apex, signal intensities on diffusion-weighted imaging are also low [40]. An overview of intensities on various sequences of the most frequent lesions and pseudolesions of the petrous apex is given in Table 1.

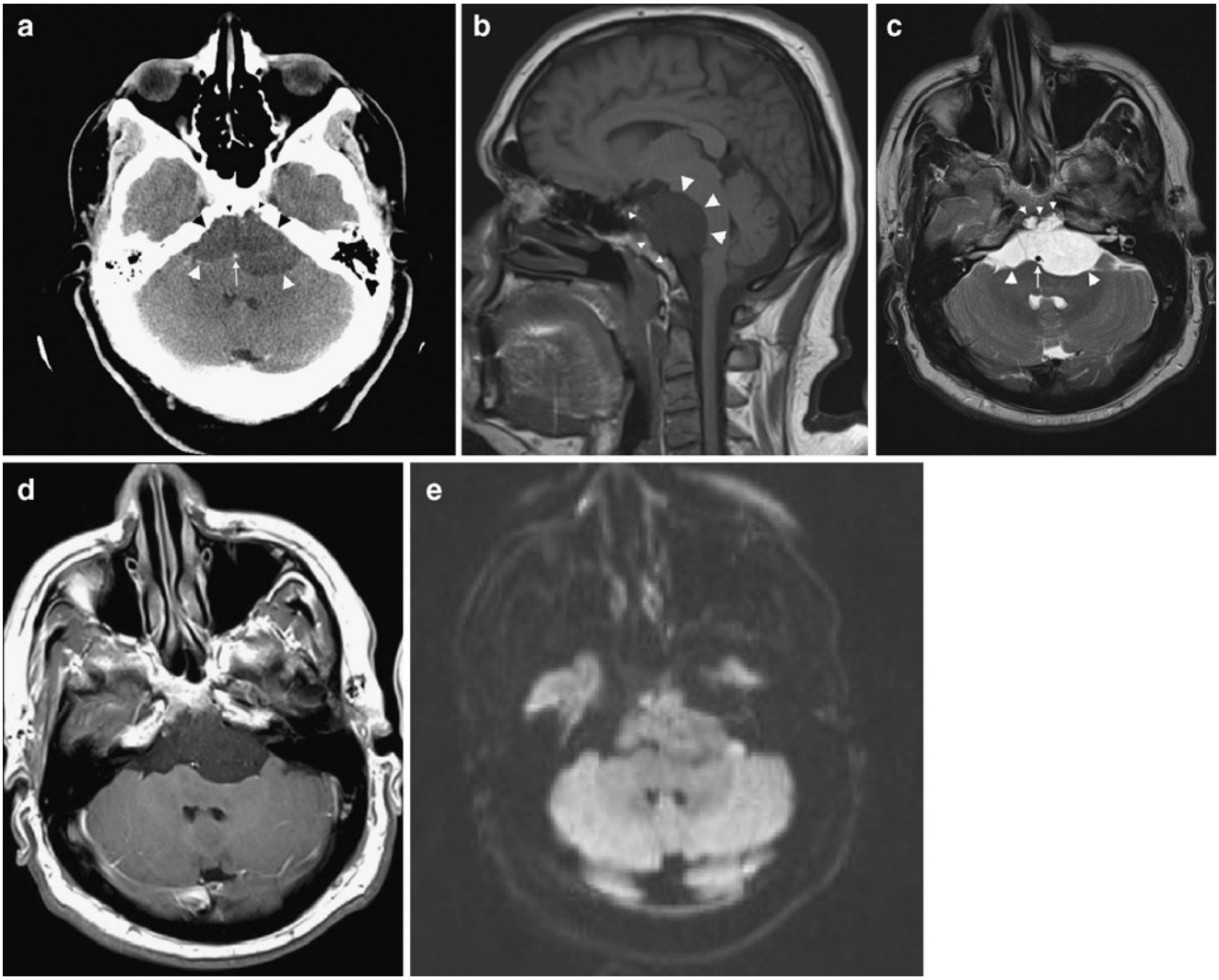

Fig. 19 A 43-year-old male presenting with headache. **a** Axial contrast enhanced CT scan through the posterior fossa. There is a large hypodense lesion (*large arrowheads*) in the prepontine cistern, encasing the basilar artery (*arrow*). Note the irregular bony delineation of the clivus (*small arrowheads*). **b** Sagittal SE T1-weighted. There is a large hypointense lesion in the prepontine cistern, compressing the brain stem (*large arrowheads*). Note the relation to the clivus. The latter is partially hyperintense due to the fat and partially hypointense due to invasion by the lesion (*small arrowheads*). **c** Axial TSE T2-weighted image through the posterior fossa (same level as **a**). Large hyperintense mass lesion in the prepontine cistern with compression of the brainstem and cerebellum (*large arrowheads*), encasing the basilar artery (*arrow*). Note again the relationship with the clivus (*small arrowheads*). **d** Axial gadolinium-enhanced SE T1-weighted image through the posterior fossa (same level as **a** and **c**). The lesion does not enhance. **e** Axial non-EP DW b1000 image (SS TSE DW sequence or HASTE DW sequence). The lesion is isointense with the cerebellum. There is no clear hyperintensity. Conclusion: The large mass lesion displays signal intensities on standard MR sequences which might be compatible with an epidermoid cyst. However, the lack of clear hyperintensity on b1000 diffusion-weighted images and the relation to the clivus disfavour the diagnosis of an epidermoid cyst. At surgery, pathology revealed a chordoma. The clue to the diagnosis is indeed given by the relation of the lesion to the clivus

CPA lesions

The scala of CPA lesions is large and diverse and is beyond the scope of this paper. The top three of space occupying lesions in the cerebello-pontine angle are vestibule-cochlear schwannoma, meningeoma, and epidermoid cyst [41, 42].

The biggest group consists of vestibulo-cochlear schwannomas and meningeomas, accounting for about 90% of all tumorous lesions of the CPA. Both lesions display an isointensity to brain on unenhanced T1-weighted images, have a slight hyperintensity on T2-weighted images, and demonstrate a clear enhancement on post-gadolinium T1-weighted images. Vestibulo-cochlear schwannomas are always situated in the course of the vestibulo-cochlear nerve with often a component inside the internal auditory canal (IAC) and a component protruding in the CPA. The CPA component has sharp angles with the posteromedial surface of the temporal bone and can rarely display a dural tail [41, 42].

The meningeoma is usually eccentric to the IAC, but it may cover the IAC and even extend into the IAC. It has obtuse angles with the posteromedial surface of the temporal bone and displays a dural tail caused by either tumorous infiltration either caused by inflammatory changes [41, 42].

The epidermoid inclusion cyst is the third most common lesion of the CPA, accounting for about 5% of all mass lesions in the CPA. It can have a supratentorial extension with components into the middle cranial fossa, Meckel's cave, the suprasellar region, and the quadrigeminal plate cistern. It is considered a congenital lesion rather than a tumoral lesion originating at the time of closure of the neural tube. It is a slowly growing mass due to continuous desquamation of the lining epithelium. Symptoms are usually caused due to compression of cranial nerves, the brain stem, and/or the cerebellum [42].

The epidermoid inclusion cyst has as a CSF-like appearance on standard MRI sequences, looking isointense on T1-weighted images and hyperintense on T2-weighted images. On these sequences, differentiation with an arachnoid cyst is very difficult. Arachnoid cysts are frequent in the CPA and can have a compressive effect on the 7th and 8th cranial nerve or on the 9th, 10th, and 11th cranial nerve depending on its location. Arachnoid cysts also have a CSF-like appearance.

On heavily T2-weighted sequences and fluid-attenuated inversion recovery (FLAIR) sequences, arachnoid cysts still have CSF appearance whereas epidermoid inclusion cysts have a mixed hyper–hypointense appearance on these heavily T2-weighted sequences and an inhomogeneous hyperintense appearance on FLAIR sequences. The appearance on heavily T2-weighted sequences and FLAIR sequences is caused by the fact that an epidermoid cyst is constituted of lamellated desquamated keratin. Diffusion-weighted imaging clearly shows a hyperintense signal intensity in case of an epidermoid inclusion cyst as epidermoid inclusion cysts are histologically exactly the same as acquired or congenital cholesteatoma (Fig. 16). Arachnoid cysts do not display hyperintensity on diffusion-weighted images [42, 43] (Fig. 17).

Non-EP diffusion-weighted sequences are to be preferred over EP diffusion-weighted sequences because of their lack of susceptibility artefacts.

Diffusion-weighted sequences are also crucial in the postoperative follow-up as it allows confirmation of the presence of a possible residual tumor [42] (Fig. 18).

In the evaluation of a CPA lesion, a diffusion-weighted sequence should always be included. It narrows differential diagnosis in lesions in which standard MR sequences are not equivocal (Fig. 19).

Conflict of interest We declare that we have no conflict of interest.

References

1. Thoeny HC, Keyzer D (2007) Extracranial applications of diffusion-weighted magnetic resonance imaging. Eur Radiol 17:1385–1393
2. Bammer R, Holdsworth SJ, Veldhuis WB, Skare ST (2009) New methods in diffusion-weighted and diffusion tensor imaging. Magn Reson Imaging Clin N Am 17:175–204
3. De Foer B, Vercruysse JP, Pilet B et al (2006) Single-shot, turbo spin-echo, diffusion-weighted imaging versus spin-echo planar, diffusion-weighted imaging in the detection of acquired middle ear cholesteatoma. ANJR Am J Neuroradiol 27:1480–1482
4. Dubrulle F, Souillard R, Chechin D et al (2006) Diffusion-weighted MR imaging sequence in the detection of postoperative recurrent cholesteatoma. Radiology 238:604–610
5. Lehmann P, Saliou G, Brochart C et al (2009) 3 T MR imaging of postoperative recurrent middle ear cholesteatomas: value of periodically rotated overlapping parallel lines with enhanced reconstruction diffusion-weighted MR imaging. AJNR Am J Neuroradiol 30:423–427
6. Nelson M, Roger G, Koltai PJ et al (2002) Congenital cholesteatoma: classification, management and outcome. Arch Otolaryngol Head Neck Surg 128:810–814
7. Kutz JW Jr, Friedman RA (2007) Congenital middle ear cholesteatoma. Ear Nose Throat J 86:654
8. Lemmerling M, De Foer B (2004) Imaging of cholesteatomatous and non-cholesteatomatouvarga, cholesteatomas middle ear disease. In: Lemmerling M, Kollias SS (eds) Radiology of the petrous bone. Springer, New York, pp 31–47
9. Barath K, Huber AM, Stämpfli P, Varga P, Kollias S (2010) Neuroradiology of cholesteatomas. AJNR Am J Neuroradiol Apr 1 (Epub ahead of print).
10. Brown JS (1982) A ten year statistical follow-up of 1142 consecutive cases of cholesteatoma: the closed versus the open technique. Laryngoscope 92:390–396

11. Schilder AG, Govaerts PJ, Somers T, Offeciers FE (1997) Tympano-ossicular allografts for cholesteatoma in children. Int J Pediatr Otorhinolaryngol 42:31–40
12. Mercke U (1987) The cholesteatomatous ear one year after surgery with obliteration technique. Am J Otol 8:534–536
13. Gantz BJ, Wilkinson EP, Hansen MR (2005) Canal wall reconstruction tympanomastoidectomy with mastoid obliteration. Laryngoscope 115:1734–1740
14. Offeciers E, Vercruysse JP, De Foer B, Casselman J, Somers T (2008) Mastoid and epitympanic obliteration. The obliteration technique. In: Ars B (ed) Chronic otitis media. Pathogenesis oriented therapeutic treatment. Kugler, Amsterdam, pp 299–327
15. Vercruysse JP, De Foer B, Somers T, Casselman JW, Offeciers E (2008) Mastoid and epitympanic bony obliteration in pediatric cholesteatoma. Otol Neurotol 29:953–960
16. Martin N, Sterkers O, Nahum (1990) Chronic inflammatory disease of the middle ear cavities: Gd-DTPA-enhanced MR imaging. Radiology 176:39–405
17. Fitzek C, Mewes T, Fitzek S et al (2002) Diffusion-weighted MRI of cholesteatomas of the petrous bone. J Magn Reson Imaging 15:636–641
18. Vercruysse JP, De Foer B, Pouillon M et al (2006) The value of diffusion-weighted MR imaging in the diagnosis of primary acquired and residual cholesteatoma: a surgical verified study of 100 patients. Eur Radiol 16:1461–1467
19. De Foer B, Vercruysse JP, Bernaerts A et al (2007) The value of single-shot turbo spin-echo diffusion-weighted MR imaging in the detection of middle ear cholesteatoma. Neuroradiology 49:841–848
20. 7Lemmerling MM, De Foer B, VandeVyver V, Vercruysse JP, Kl V (2008) Imaging of the opacified middle ear. Eur J Radiol 66:363–371
21. Lemmerling MM, De Foer B, Verbist BM, VandeVyver V (2009) Imaging of inflammatory and infectious diseases in the temporal bone. Neuroimaging Clin N Am 19:321–337
22. De Foer B, Vercruysse JP, Bernaerts A et al (2010) Middle ear cholesteatoma: non-echo-planar diffusion-weighted MR imaging versus delayed gadolinium-enhanced T1-weighted MR—value in detection. Radiology 255:866–872
23. Venail F, Bonafe A, Poirrier V, Mondain M, Uziel A (2008) Comparison of echo-planar diffusion-weighted imaging and delayed postcontrast T1-weighted MR imaging for the detection of residual cholesteatoma. AJNR Am J Neuroradiol 29:1363–1368
24. Jeunen G, Desloovere C, Hermans R, Vandecavye V (2008) The value of magnetic resonance imaging in the diagnosis of residual or recurrent acquired cholesteatoma after canal wall-up tympanoplasty. Otol Neurotol 29:16–18
25. Sheehy JL, Brackman DE, Graham MD (1977) Cholesteatoma surgery: residual and recurrent disease. A review of 1024 cases. Ann Otol Rhinol Laryngol 86:451–462
26. Brackman DE (1993) Tympanoplasty with mastoidectomy: canal wall up procedures. Am J Otol 14:380–382
27. Vanden Abeele D, Coen E, Parizel PM, Van de Heyning P (1999) Can MRI replace a second look operation in cholesteatoma surgery? Acta Otolaryngol 119:555–561
28. Williams MT, Ayache D, Albert C et al (2003) Detection of postoperative residual cholesteatoma with delayed contrast-enhanced MR imaging: initial findings. Eur Radiol 13:169–174
29. Ayache D, Williams MT, Lejeune D, Corré A (2005) Usefulness of delayed postcontrast magnetic resonance imaging in the detection of residual cholesteatoma after canal wall-up tympanoplasty. Laryngoscope 115:607–610
30. Aikele P, Kittner T, Offergeld C et al (2003) Diffusion-weighted MR imaging of cholesteatoma tin pediatric and adult patients who have undergone middle ear surgery. AJR Am J Roentgenol 181:261–265
31. Stasolla A, Magliulo G, Parrotto D, Luppi G, Marini M (2004) Detection of postoperative relapsing/residual cholesteatoma with diffusion-weighted echo-planar magnetic resonance imaging. Otol Neurotol 25:879–884
32. De Foer B, Vercruysse JP, Bernaert A et al (2008) Detection of postoperative residual cholesteatoma with non-echo-planar diffusion-weighted magnetic resonance imaging. Otol Neurotol 29:513–517
33. Dhenpnorrarat RC, Wood B, Rajan GP (2009) Postoperative non-echo-planar diffusion-weighted magnetic resonance imaging changes after cholesteatoma surgery: implications for cholesteatoma screening. Otol Neurotol 30:54–58
34. Rajan GP, Ambett R, Wun L et al (2010) Preliminary outcomes of cholesteatoma screening in children using non-echo-planar diffusion-weighted magnetic resonance imaging. Int J Pediatr Otorhinolaryngol 74:297–301
35. De Foer B, Vercruysse JP, Pouillon M et al (2007) Value of high-resolution computed tomography and magnetic resonance imaging in the detection of residual cholesteatoma in primary bony obliterated mastoids. Am J Otolaryngol 28:230–234
36. Vercruysse JP, De Foer B, Somers T, Casselman J, Offeciers E (2010) Lont-term follow up after bony mastoid and epitympanic obliteration: radiological findings. J Laryngol Otol 124:37–43
37. Lemmerling M (2004) Petrous apex lesions. In: Lemmerling M, Kollias SS (eds) Radiology of the petrous bone. Springer, New York, pp 171–179
38. Schmalfuss IM (2009) Petrous apex. Neuroimaging Clin N Am 19:367–391
39. Silveira Filho LG, Ayache D, Sterkers O, Williams MT (2010) Middle ear cholesteatoma extending into the petrous apex. Otol Neurotol 31:544–545
40. Alkilic-Genauzeau I, Boukobza M, Lot G, George B, Merland JJ (2007) CT and MRI features of arachnoid cyst of the petrous apex: report of 3 cases. J Radiol 88:1179–1183
41. Bonneville SJ, Chiras J (2007) Imaging of cerebellopontine angle lesions: an update. Part 1: enhancing extra-axial lesions. Eur Radiol 17:2472–2482
42. Bonneville F, Savatovsky J, Chiras J (2007) Imaging of cerebellopontine angle lesions: an update. Part 2: intra-axial lesions, skull base lesions that may invade the CPA region, and non-enhancing extra-axial lesions. Eur Radiol 17:2908–2920
43. Liu P, Saida Y, Yoshioka H, Itai Y (2003) MR imaging of epidermoids at the cerebellopontine angle. Magn Reson Med Sci 2:109–115